Supplementary Material for

A Bihormonal Closed-Loop Artificial Pancreas for Type 1 Diabetes

Firas H. El-Khatib, Steven J. Russell*, David M. Nathan, Robert G. Sutherlin, Edward R. Damiano

*To whom correspondence should be addressed. E-mail: sjrussell@partners.org

This PDF file includes:

Methods
Fig. S1. Depiction of the bihormonal closed-loop control system used in the clinical trial.
Fig. S2. First closed-loop experiment in #108 using controller with fast PK parameter settings.
Fig. S3. First closed-loop experiment in #110 using controller with fast PK parameter settings.
Fig. S4. First closed-loop experiment in #117 using controller with fast PK parameter settings.
Fig. S5. First closed-loop experiment in #119 using controller with fast PK parameter settings.
Fig. S6. First closed-loop experiment in #126 using controller with fast PK parameter settings.
Fig. S7. First closed-loop experiment in #128 using controller with fast PK parameter settings.
Fig. S8. First closed-loop experiment in #115 using controller with fast PK parameter settings.
Fig. S9. First closed-loop experiment in #121 using controller with fast PK parameter settings.
Fig. S10. First closed-loop experiment in #122 using controller with fast PK parameter settings.
Fig. S11. First closed-loop experiment in #129 using controller with fast PK parameter settings.
Fig. S12. First closed-loop experiment in #132 using controller with fast PK parameter settings.
Fig. S13. Second closed-loop experiment in #115 using controller with slow PK parameter settings.
Fig. S14. Second closed-loop experiment in #121 using controller with slow PK parameter settings.
Fig. S15. Second closed-loop experiment in #122 using controller with slow PK parameter settings.
Fig. S16. Second closed-loop experiment in #129 using controller with slow PK parameter settings.
Fig. S17. Second closed-loop experiment in #132 using controller with slow PK parameter settings.
Fig. S18. Second closed-loop experiment in #110 using controller with slow PK parameter settings.
Fig. S19. Second closed-loop experiment in #117 using controller with slow PK parameter settings.
Fig. S20. Second closed-loop experiment in #126 using controller with slow PK parameter settings.
Fig. S21. Second closed-loop experiment in #128 using controller with slow PK parameter settings.
References and Notes

METHODS

SOM Note 1: Control algorithm for insulin administration

Empirical subject model

An empirical form is adopted for the subject model, with a single-input single-output (SISO) auto-regressive moving average with exogenous (ARMAX) input structure, namely

$$A(z^{-1})\, y_t = z^{-d}\, B(z^{-1})\, u_t + C(z^{-1})\, w_t, \tag{1}$$

where u_t denotes the (input) insulin dose, y_t denotes the (output) glucose concentration deviation from the reference set point, w_t is a white Gaussian noise sequence, d is the inherent system time-delay (dead-time), z^{-1} plays the role of the unit delay shift operator, and the scalar polynomials A, B, and C are given by

$$\begin{aligned} A(z^{-1}) &= 1 + a_1\, z^{-1} + a_2\, z^{-2} + \ldots + a_n\, z^{-n}, \\ B(z^{-1}) &= b_0 + b_1\, z^{-1} + b_2\, z^{-2} + \ldots + b_m\, z^{-m}, \\ C(z^{-1}) &= 1 + c_1\, z^{-1} + c_2\, z^{-2} + \ldots + c_p\, z^{-p}. \end{aligned}$$

The model's orders and delay may be determined beforehand from offline system identification analysis (*1*). The model is then employed online in the integrated control system, whereby the model parameters are recursively updated online (*2–4*), by first re-writing the model in regressor form (*5*), namely

$$y_t = \theta^T\, \psi_t + w_t, \tag{2}$$

where the regressor, ψ_t, and parameter vector, θ, are respectively given by

$$\begin{aligned} \psi_t &:= [\, -y_{t-1} \ldots -y_{t-n}\; u_{t-d} \ldots u_{t-d-m}\; w_{t-1} \ldots w_{t-p}\,]^T, \\ \theta &:= [\, a_1 \ldots a_n\; b_0 \ldots b_m\; c_1 \ldots c_p\,]^T. \end{aligned} \tag{3}$$

With online parameter estimates packed in a time-varying version of vector θ, namely θ_t, and the estimate $\hat{w}_t := y_t - \psi_t^T\, \theta_t$ used in lieu of w_t in ψ_t, the extended least-squares (ELS) method described by Lai and Wei (*5, 6*) follows the scheme

$$\theta_t = \theta_{t-1} + \frac{P_{t-1}\, \psi_t}{1 + \psi_t^T\, P_{t-1}\, \psi_t}\, e_t, \tag{4}$$

$$P_t = P_{t-1} - \frac{P_{t-1}\, \psi_t\, \psi_t^T\, P_{t-1}}{1 + \psi_t^T\, P_{t-1}\, \psi_t}, \tag{5}$$

where $e_t := y_t - \psi_t^T\, \theta_{t-1}$, and P_0 is taken to be a positive definite matrix. As such, the subject model parameters can be recursively estimated in realtime and passed to the online control algorithm, thereby providing an indirect adaptive control strategy (*2, 3, 6, 7*).

Generalized predictive control

Basic predictive control

For the online glucose control algorithm, we propose generalized predictive control (GPC), which optimizes the multi-stage quadratic cost function (*7, 8*) given by

$$J_{\text{GPC}} = \sum_{k=N_d}^{N_m} \delta_k\, ||C\,(r_{t+k} - y_{t+k})||^2 \; + \sum_{k=0}^{N_u} \lambda_k\, (\Delta u_{t+k})^2, \tag{6}$$

where N_d and N_m are respectively the minimum and maximum (output) prediction costing horizon limits, N_u the control horizon bound, δ_m the weighting on prediction error, and λ_n the weighting on control signals. For control action with integral effect (*7, 9*), predictor formulation and control design are based on

$$A(z^{-1})\, y_t = z^{-k}\, B(z^{-1})\, u_t + C(z^{-1})\, w_t/\Delta, \tag{7}$$

with the corresponding Diophantine separation identity (*6, 7*) given by

$$\frac{C}{A\Delta} = E_k + z^{-k}\, \frac{F_k}{A\Delta}, \tag{8}$$

where F_k is the remainder polynomial corresponding to the *monic* quotient polynomial E_k, the former and latter being of respective orders n and $k-1$ in z^{-1}, or, specifically, $F_k = f_0 + f_1\, z^{-1} + ... + f_n\, z^{-n}$ and $E_k = 1 + e_1\, z^{-1} + ... + e_{k-1}\, z^{-(k-1)}$. The best predictor $\hat{y}_{t|t-k}$ is then defined (*6, 7*) to satisfy

$$y_t = \hat{y}_{t|t-k} + E_k\, w_t, \tag{9}$$

which yields

$$C\, \hat{y}_{t+k|t} = G_k\, \Delta\, u_{t+k-d} + F_k\, y_t, \tag{10}$$

where $G_k := E_k B$. Note that G_k is order 'm+$k-1$' in z^{-1}, and can be written as $G_k = g_0 + g_1\, z^{-1} + ... + g_{m+k-1}\, z^{-(m+k-1)}$, with $g_0 = b_0$, since E_k is monic for all k. To implement the GPC aglorithm (*6–8*), we re-write Eq. (10) as

$$C\, \hat{y}_{t+k|t} = \sum_{i=0}^{k-d} g_i\, z^{-i} \Delta\, u_{t+k-d} + (G_k - \sum_{i=0}^{k-d} g_i\, z^{-i})\, \Delta\, u_{t+k-d} + F_k\, y_t, \tag{11}$$

where the first term on the right-hand side contains the only $k-d$ future-terms (containing the sought control signal) for any k. Taking $N_d = d$ and $N_y + 1 = N_u + 1 =: N$, i.e. square prediction and control horizons of N steps, we apply this over $k = d \rightarrow (N_y + d)$, and pack term contributions in the matrix-form equation given by

$$\boldsymbol{y} = \boldsymbol{G}\, \boldsymbol{u} + \boldsymbol{G'}\boldsymbol{u} + \boldsymbol{F}\, y_t, \tag{12}$$

where

$$\boldsymbol{y} = \begin{bmatrix} C\, \hat{y}_{t+d|t} \\ C\, \hat{y}_{t+d+1|t} \\ . \\ . \\ . \\ C\, \hat{y}_{t+N+d-1|t} \end{bmatrix}_{N\times 1} \qquad \boldsymbol{u} = \begin{bmatrix} \Delta\, u_t \\ \Delta\, u_{t+1} \\ . \\ . \\ . \\ \Delta\, u_{t+N-1} \end{bmatrix}_{N\times 1}$$

$$\boldsymbol{G} = \begin{bmatrix} g_0 & 0 & 0 & . & . & . \\ g_1 & g_0 & 0 & . & . & . \\ . & . & . & . & . & . \\ . & . & . & . & . & . \\ . & . & . & . & . & 0 \\ g_{N-1} & g_{N-2} & . & . & . & g_0 \end{bmatrix}_{N\times N}$$

$$\boldsymbol{G'u} = \begin{bmatrix} (G_d - \sum_{i=0}^{0} g_i\, z^{-i})\, \Delta\, u_t \\ (G_{d+1} - \sum_{i=0}^{1} g_i\, z^{-i})\, \Delta\, u_{t+1} \\ . \\ . \\ . \\ (G_{N+d-1} - \sum_{i=0}^{N-1} g_i\, z^{-i})\, \Delta\, u_{t+N-1} \end{bmatrix}_{N\times 1}$$

and

$$\boldsymbol{F} = \begin{bmatrix} F_d \\ F_{d+1} \\ \cdot \\ \cdot \\ \cdot \\ F_{N+d-1} \end{bmatrix}_{N\times 1}.$$

The last two quantities in Eq. (12) are available at time t, as they are either directly measurable or depend only on past measurements, and can be grouped into a vector $\boldsymbol{f}$, leading to

$$\boldsymbol{y} = \boldsymbol{G}\,\boldsymbol{u} + \boldsymbol{f}. \tag{13}$$

With $\delta_m = 1$ and $\lambda_n = \lambda$, Eq. (6) can be re-written as

$$J_{\text{GPC}} = (\boldsymbol{G} + \boldsymbol{f} - \boldsymbol{r})^T\,(\boldsymbol{G} + \boldsymbol{f} - \boldsymbol{r}) + \lambda \boldsymbol{u}^T\boldsymbol{u}, \tag{14}$$

where $\boldsymbol{r}$ is the vector holding future set points, namely $\boldsymbol{r} = [C\,r_{t+d}\;\; C\,r_{t+d+1}\;...\;C\,r_{t+N+d-1}]^T$. Further manipulation of Eq. (14) leads to

$$J_{\text{GPC}} = \tfrac{1}{2}\,\boldsymbol{u}^T\boldsymbol{H}\boldsymbol{u} + \boldsymbol{b}^T\boldsymbol{u} + \boldsymbol{f}_0, \tag{15}$$

where

$$\boldsymbol{H} = 2(\boldsymbol{G}^T\boldsymbol{G} + \lambda\boldsymbol{I}), \quad \boldsymbol{b}^T = 2(\boldsymbol{f} - \boldsymbol{r})^T\boldsymbol{G},$$

and

$$\boldsymbol{f}_0 = (\boldsymbol{f} - \boldsymbol{r})^T\,(\boldsymbol{f} - \boldsymbol{r}).$$

The unconstrained vector $\boldsymbol{u}$ minimizing J_{GPC} can be found by inspection (*7*) of Eq. (15), and is given by

$$\boldsymbol{u}_{\text{GPC}} = -\boldsymbol{H}^{-1}\boldsymbol{b} = (\boldsymbol{G}^T\boldsymbol{G} + \lambda\boldsymbol{I})^{-1}\boldsymbol{G}^T(\boldsymbol{r} - \boldsymbol{f}). \tag{16}$$

Since $\boldsymbol{G}^T\boldsymbol{G} \geq \boldsymbol{0}$, Eq. (16) gives a unique solution, provided $\lambda > 0$. Only the first control move is of interest at t, namely

$$\Delta u_t = [\,1\;0\;0\;...\;0\,]\,(\boldsymbol{G}^T\boldsymbol{G} + \lambda\boldsymbol{I})^{-1}\boldsymbol{G}^T(\boldsymbol{r} - \boldsymbol{f}). \tag{17}$$

The control increment or move in Eq. (17) is thus zero if the current setting and desired outcome coincide, that is if $\boldsymbol{r} - \boldsymbol{f} = \boldsymbol{0}$, as it should (*7*). Finally, to deal with non-square horizons, which would only be permissible for $N_u < N_y$, $\boldsymbol{G}$ is replaced by $\boldsymbol{G}_{Nu}$, where $\boldsymbol{G}_{Nu}$ is composed of the first N_u+1 columns of $\boldsymbol{G}$, and $\boldsymbol{u}$ is replaced by $\boldsymbol{u}_{Nu}$, which contains the first N_u+1 elements of $\boldsymbol{u}$, with everything else kept the same (*7*). Note that the generalized minimum variance (GMV) control, with $N_y = N_u = N - 1 = 0$, is a special instance of GPC with square horizons (*2, 3, 10*).

Augmented control algorithm

Since excessive accumulation of insulin in the subcutaneous (SC) tissue (or in blood/plasma) could be detrimental, and since such accumulation essentially depends on the input control signal, it can be augmented to the raw control cost function of Eq. (6), with its minimization viewed as an additional control objective in the optimization process. The resultant online control signal will therefore simultaneously (i) optmize the controller's aggressiveness, (ii) minimize insulin accumulation in the SC depot (and in plasma), and (iii) regulate glucose concentration to a preset set point. The mathematical formulation governing the SC (and plasma) accumulation of exogenous insulin can be derived based on nominal temporal values pertaining to its pharmacokinetics, i.e. its time-course of activity from SC tissue into plasma, in terms of its absorption rate, peak absorption time, and overall time of action (perfusion into plasma). This has already been analyzed in the literature (*11*) and the permeation of insulin from the SC tissue into plasma is known to possess a typical profile, with the nominal values of its characteristic parameters being predominantly dependent on the kind of insulin used. If $p(t)$ is the concentration, measured in U/dl, of insulin in plasma as it is absorbed from the SC depot (*12*), the pharmacokinetics of fast-acting insulin (*11, 13*) suggest that its evolution in plasma can be governed by

$$p(t) = K\,U_0\,(e^{-\alpha_1 t} - e^{-\alpha_2 t}). \tag{18}$$

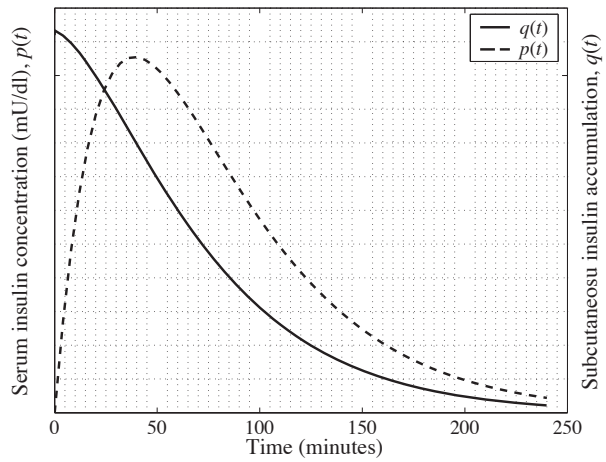

Ad-hoc superposition of the concentration, $p(t)$, of serum insulin in plasma (dashed), in accordance with Eq. (18), and outstanding accumulation, $q(t)$, of insulin in the subcutaneous depot (solid), in accordance with Eq. (19), following an impulse exogenous dose into the SC tissue.

where U_0 is the subcutaneous-drug impulse dose in units (U), K is a constant, in dl^{-1}, associated with the amplitude of the impulse response of $p(t)$, and α_1 and α_2 are positive constants in min^{-1} (or s^{-1}, depending on t). The latter three constants can all be identified from values of the peak absorption time, the peak absorption concentration, and the overall time of action associated with the pharmacokinetics of insulin, which depends on the the type of insulin used. A measure of the pending effect of the accumulated amount of insulin in the SC depot can be taken to be the difference between the total area ($\int_0^\infty p(\tau)\,\mathrm{d}\tau$, i.e. a measure of the total action over time due to dose U_0) and $\int_0^t p(\tau)\,\mathrm{d}\tau$, i.e. a measure of the expended portion of U_0. With the measure of the outstanding quantity of insulin in the SC depot, denoted by $q(t)$, we arrive at

$$q(t) = \int_t^\infty p(\tau)\,\mathrm{d}\tau = \frac{K\,U_0}{\alpha_1\,\alpha_2}\,(\alpha_2\,e^{-\alpha_1 t} - \alpha_1\,e^{-\alpha_2 t}), \tag{19}$$

which is shown in the figure above superimposed on $p(t)$ for nominal values of the parameters α_1, α_2, U_0, and K.

Assuming a delay of d_q in detecting the SC accumulation and plasma effect following exogenous administration, the discrete-time equivalent of Eqs. (18) and (19) can be written as

$$\begin{aligned} p_k &= (e^{-\alpha_1 T_s} + e^{-\alpha_2 T_s})p_{k-1} - e^{-(\alpha_1+\alpha_2)T_s}p_{k-2} + 0\,u_{k-d_q} + K\,(e^{-\alpha_1 T_s} - e^{-\alpha_2 T_s})u_{k-d_q-1} \\ &=: -a_{1p}\,p_{k-1} - a_{2p}\,p_{k-2} + b_{0p}\,u_{k-d_q} + b_{1p}\,u_{k-d_q-1}\,, \quad b_{ij}=0\ \forall\, u_j \geq 0 \end{aligned} \tag{20}$$

$$\begin{aligned} q_k &= (e^{-\alpha_1 T_s} + e^{-\alpha_2 T_s})q_{k-1} - e^{-(\alpha_1+\alpha_2)T_s}q_{k-2} + \frac{K}{\alpha_1\,\alpha_2}\,(\alpha_2 - \alpha_1)u_{k-d_q} \\ &\quad + \frac{K}{\alpha_1\,\alpha_2}\,(\alpha_1\,e^{-\alpha_1 T_s} - \alpha_2\,e^{-\alpha_2 T_s})u_{k-d_q-1} \\ &=: -a_{1q}\,q_{k-1} - a_{2q}\,q_{k-2} + b_{0q}\,u_{k-d_q} + b_{1q}\,u_{k-d_q-1}\,, \quad b_{ij}=0\ \forall\, u_j \geq 0 \end{aligned} \tag{21}$$

where T_s is the sampling period.

Before augmenting Eqs. (20) and (21) to the original discrete-time model of Eq. (1), whose inherent units are mg/dl, we re-scale both equations to switch their inherent units from U/dl and U min/dl (respectively) to mg/dl, so that the computation (optimization) of the control signal is performed on an overall homogenous (augmented) system. Such scaling factors can be defined by $s_p = (\bar{y}/U_0)/K$ and $s_q = (\alpha_1\,\alpha_2/(\alpha_2 - \alpha_1))\,(\bar{y}/U_0)/K$, where $\bar{y}/U_0$ is the average blood-glucose excursion per time step (offset from reference) per unit input, U_0. The value of $\bar{y}/U_0$ can be viewed as an "augmentation factor" (or augmentation ratio relative to the y_k-system), the range of which can be estimated by testing the augmented algorithm in closed-loop glucose-control experiments. This quantity is a key tuning knob that strongly determines the aggressiveness or conservativeness of the augmented control algorithm.

Upon scaling, a combined quantity can be conveniently defined as $\Phi_k := s_p\, p_k + s_q\, q_k$, which is then augmented to the original y_k system of Eq. (1), thereby obtaining the single-input multiple-output model given by

$$\boldsymbol{A}(z^{-1})\, \boldsymbol{y}_k = z^{-d}\, \boldsymbol{B}(z^{-1})\, u_k + \boldsymbol{C}(z^{-1})\, \boldsymbol{w}_k, \tag{22}$$

where $\boldsymbol{y}_k = [y_k \;\; \Phi_k]^T$, $\boldsymbol{w}_k$ is a vector of two white-noise sequences, and

$$\begin{aligned}
\boldsymbol{A}(z^{-1}) &= \boldsymbol{I} + \boldsymbol{A}_1\, z^{-1} + \boldsymbol{A}_2\, z^{-2} + ... + \boldsymbol{A}_n\, z^{-n}, \\
\boldsymbol{B}(z^{-1}) &= \boldsymbol{B}_0 + \boldsymbol{B}_1\, z^{-1} + \boldsymbol{B}_2\, z^{-2} + ... + \boldsymbol{B}_m\, z^{-m}, \\
\boldsymbol{C}(z^{-1}) &= \boldsymbol{I} + \boldsymbol{C}_1\, z^{-1} + \boldsymbol{C}_2\, z^{-2} + ... + \boldsymbol{C}_p\, z^{-p},
\end{aligned}$$

with

$$\boldsymbol{A}_1 = \begin{bmatrix} a_1 & 0 \\ 0 & a_{1q} \end{bmatrix}, \quad \boldsymbol{A}_2 = \begin{bmatrix} a_i & 0 \\ 0 & a_{2q} \end{bmatrix},$$

$$\boldsymbol{A}_i = \begin{bmatrix} a_i & 0 \\ 0 & 0 \end{bmatrix}, \;\; \forall\, i > 2,$$

$$\boldsymbol{B}_0 = \begin{bmatrix} b_0 \\ s_p\, b_{0p} + s_q\, b_{0q} \end{bmatrix}, \quad \boldsymbol{B}_1 = \begin{bmatrix} b_1 \\ s_p\, b_{1p} + s_q\, b_{1q} \end{bmatrix},$$

$$\boldsymbol{B}_i = \begin{bmatrix} b_i \\ 0 \end{bmatrix}, \;\; \forall\, i > 1, \quad \boldsymbol{C}_i = \begin{bmatrix} c_i & 0 \\ 0 & 0 \end{bmatrix} \;\; \forall\, i > 0,$$

and $\boldsymbol{I}$ is the 2×2 identity matrix. For simplicity, the same system delay, d, of Eq. (1) can be assumed between u_k and both p_k and q_k (i.e. $dq = d$). Since the multiple-output system is diagonal in $\boldsymbol{A}(z^{-1})$ and $\boldsymbol{C}(z^{-1})$, the y_k- and Φ_k-systems can be decoupled as far as parameter adaptation for the y_k-system is concerned (the Φ_k-system being static) (*7*). The ramifications of augmenting the Φ_k-system are also minimal in terms of the procedure for control signal computation (*7*), since separate Diophantine identities can be handled for the y_k- and Φ_k-systems. Coupling between the two systems, via the same input signal, is relevant when solving for the optimal control signal (*7*), whereby the matrix $\boldsymbol{G}$ is merely extended to give an analogous matrix, $\boldsymbol{G}_e$, for the new system, constructed as

$$\boldsymbol{G}_e = \begin{bmatrix}
g_0 & 0 & 0 & . & . & . \\
g_{0\Phi} & 0 & 0 & . & . & . \\
g_1 & g_0 & 0 & . & . & . \\
g_{1\Phi} & g_{0\Phi} & 0 & . & . & . \\
. & . & . & . & . & . \\
. & . & . & . & . & . \\
. & . & . & . & . & 0 \\
g_{N-1} & g_{N-2} & . & . & . & g_0 \\
g_{(N-1)\Phi} & g_{(N-2)\Phi} & . & . & . & g_{0\Phi}
\end{bmatrix}_{2N \times N},$$

where entries $g_{i\Phi}$ pertain to the Φ_k-system, and are the analogues of entries g_i in the y_k-system. Vector $\boldsymbol{f}$ is also adjusted accordingly to yield an extended version, $\boldsymbol{f}_e$, which is twice in length. The GPC signal is again given by Eq. (17), except that $\boldsymbol{G}_e$ (or its first $N_u + 1$ columns for non-square horizons) and $\boldsymbol{f}_e$ are used in lieu of $\boldsymbol{G}$ and $\boldsymbol{f}$ respectively, in addition to using a trivially extended version, $\boldsymbol{r}_e$, for $\boldsymbol{r}$. The GMV control is recovered by setting $N_y = N_u = N - 1 = 0$.

Specialized control signal

The current settings in our control algorithm are $n = 2$, $m = 1$, $p = 0$, $N_d = d = d_q = 1$, and $\boldsymbol{r_e} = [0 \;\; 0]^T$, which yield the control signal given by

$$u_t = u_{t-1} + \frac{[\, b_0 \quad (s_p\, b_{0p} + s_q\, b_{0q})\,] \cdot (-\boldsymbol{N1} - \boldsymbol{N2})}{b_0^2 + (s_p\, b_{0p} + s_q\, b_{0q})^2 + \lambda}, \tag{23}$$

$$\boldsymbol{N1} = \begin{bmatrix} b_1\,(u_{t-1} - u_{t-2}) \\ (s_p\, b_{1p} + s_q\, b_{1q})\,(u_{t-1} - u_{t-2}) \end{bmatrix}, \tag{24}$$

$$\boldsymbol{N2} = \begin{bmatrix} (1 - a_1)\, y_t + (a_1 - a_2)\, y_{t-1} + a_2\, y_{t-2} \\ (1 - a_{1pq})\,(s_p\, p_t + s_q\, q_t) + (a_{1pq} - a_{2pq})\,(s_p\, p_{t-1} + s_q\, q_{t-1}) + a_{2pq}\,(s_p\, p_{t-2} + s_q\, q_{t-2}) \end{bmatrix}, \tag{25}$$

which, upon carrying out the dot product, becomes

$$u_t = u_{t-1} - \frac{n1 + n2}{b_0^2 + (s_p\, b_{0p} + s_q\, b_{0q})^2 + \lambda}, \tag{26}$$

$$n1 = b_0\,(b_1\,(u_{t-1} - u_{t-2}) + (1 - a_1)\, y_t + (a_1 - a_2)\, y_{t-1} + a_2\, y_{t-2}), \tag{27}$$

$$\begin{aligned} n2 = {} & (s_p\, b_{0p} + s_q\, b_{0q})\,((s_p\, b_{1p} + s_q\, b_{1q})\,(u_{t-1} - u_{t-2}) + (1 - a_{1pq})\,(s_p\, p_t + s_q\, q_t) + \\ & (a_{1pq} - a_{2pq})\,(s_p\, p_{t-1} + s_q\, q_{t-1}) + a_{2pq}\,(s_p\, p_{t-2} + s_q\, q_{t-2})), \end{aligned} \tag{28}$$

where $a_{1pq} = a_{1p} = a_{1q}$ and $a_{2pq} = a_{2p} = a_{2q}$ (as per Eqs. (20) and (21)). Upon computing the control signal of Eq. (26) at every time step, parameters a_1, a_2, b_0, and b_1 are recursively updated in accordance with the ELS algorithm of Eqs. (4) and (5). Additionally, a hard constraint, namely $|u_t| \leq u_{max}$, is enforced on the control signal during online operation, where u_{max} is the maximum allowable insulin dose at any sampling period. For consistent operation, the algorithm parameters and maximum insulin dose are set for a reference "canonical" body mass (e.g. 25 kg), and the online control signal is linearly scaled with the actual subject body mass in order to obtain the insulin dose to be delivered.

SOM Note 2: Proportional-derivative algorithm for glucagon administration

A glucagon dose is triggered whenever blood-glucose concentration falls below set point or enters normal range with a rapid descent (e.g. a descent $\geq$ 10 mg/dl per 5 min). A triggered glucagon dose is computed by the proportional-derivative (PD) algorithm as follows:

$$G_{dose}(t) = k_p\,(120 - y_t) + k_d\,(y_{t-1} - y_t)/T_s - G_{pending}(t); \qquad 0 \leq G_{dose}(t) \leq G_{max} \tag{29}$$

where G_{max} is the maximum allowable glucagon dose, t is in discrete time, k_p is the proportional gain, k_d is the derivative gain, T_s is the sampling period, and $G_{pending}$ is an estimate of pending subcutaneous glucagon from recent doses, which is deducted from G_{dose} and is computed as:

$$G_{pending}(t) = \sum_{k=1}^{90/T_s} G_{dose}(t - k) \left(\frac{1}{2}\right)^{k\,T_s/G_{1/2}} \tag{30}$$

where $G_{1/2}$ is an estimate of the average half life of subcutaneous doses of glucagon. Note that the estimate $G_{pending}(t)$ limits unnecessary subcutaneous accumulation of glucagon, and can be conservatively computed (erring on the side of having somewhat extra glucagon occasionally) by assuming a short $G_{1/2}$. A reasonable estimate for $G_{1/2}$ is $\sim$ 10 minutes, which is consistent with results from pre-clinical studies in diabetic swine (*14–16*) and with the fast glucagon t_{max} values observed in subjects with type 1 diabetes in the present study.

SOM Note 3: Inferring PK parameters from measured lispro levels

Insulin PK was approximated by a two-exponential model. In the control algorithm, the insulin PK model is discretized and augmented to an input-output empirical model that relates BG and insulin dosing. This augmentation equips the algorithm with a capability to estimate the diffusion of delivered subcutaneous insulin into blood, as well as the overall subcutaneous accumulation of insulin. Thus, in light of the evolution of BG and the history of subcutaneous doses of insulin, the insulin PK model allows the control system to determine at every time step whether to deliver more insulin or refrain.

The two time constants inherent in the two-exponential model for insulin PK represent the two key parameters for estimating the time for subcutaneous insulin to peak in blood as well as the time for its (95%) clearance from blood. Based on measured plasma-insulin levels and the subcutaneous doses of insulin that were delivered by the control system in each experiment, a least-squares (LS) approach is used to determine the two parameters that would provide the PK fit that best correlates the subcutaneous doses of insulin with the plasma-insulin levels. In the process, two-exponential PK models with identical time constants are assigned to all delivered subcutaneous doses, each from its time of delivery. The union effect from the PK models of all doses (each of a different time of origin) is then computed to provide an estimate of the aggregate appearance of insulin in blood at every time step, based on all prior doses at each time point. Starting with parameters associated with near-zero time to peak, a (squares) error is computed between insulin levels in blood that are provided by this estimate and the measured plasma-insulin levels. The time constants are progressively increased (i.e. the PK model is progressively stretched) until the minimum error (LS error) is converged upon, i.e. when a turning point in the computed error is encountered. The values for the time constants corresponding to the LS error determine the best PK fit in each experiment, and are used to approximate the time for subcutaneous insulin to peak in blood as well as the time for its (95%) clearance from blood for each subject. The optimal time constants obtained from each closed-loop experiment were also used to simulate the PK response to a hypothetical subcutaneous dose of insulin, i.e. to depict an impulse response. These simulations are superimposed in the right panels in Fig. 4 of the main text.

SOM Note 4: Exclusion criteria

Subjects were also excluded if they used medications for BG control other than insulin or medications that affected gastric motility, had a history of impaired gastric motility requiring treatment, anemia, renal insufficiency, abnormal thyroid function, elevated alanine amino transferase, untreated hypertension, coronary artery disease, heart failure, or seizures.

SOM Note 5: Macronutrition content of meals

Meals provided a total of 30 kcal/kg/day for men and 25 kcal/kg/day for women. The division of energy intake between meals followed common patterns, with 45% of the daily caloric intake occurring at dinner, 25% at breakfast, and 30% at lunch. The macronutrient content of meals was designed to provide different challenges to BG control. The percentage of calories provided as carbohydrate, protein, and fat was divided as follows: Dinner – 45%, 22.5%, 32.5%; Breakfast – 60%, 15%, 25%; Lunch – 50%, 20%, 30%. The subjects were required to finish the entire meal within 30 minutes of receiving it. Other than the meals provided, subjects were not be allowed to consume any other food items or drinks besides water or diet drinks that contain negligible calories.

SOM Note 6: Intervention criteria for hypoglycemia

Oral carbohydrates (15 g) were given for treatment of hypoglycemia if the BG was below 60 mg/dl for 4 consecutive measurements (20 min) or below 50 mg/dl for 2 consecutive measurements (10 min), or if the subject complained of hypoglycemic symptoms at any time when BG was less than 60 mg/dl. If three doses of oral carbohydrates were required in 1 hr, the protocol was discontinued and the BG was stabilized in the normal range.

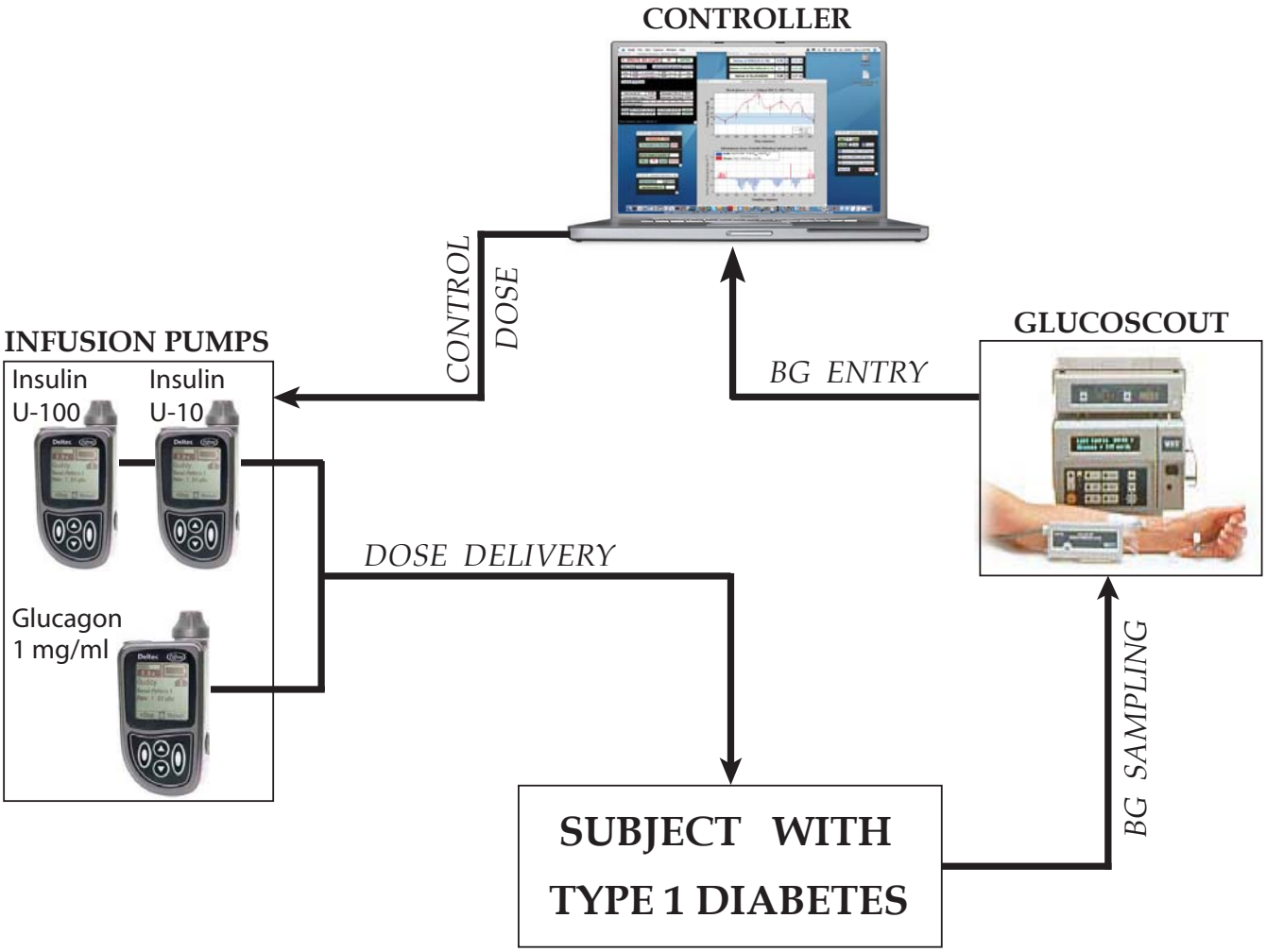

Fig. S1. Depiction of the bihormonal closed-loop control system used in the clinical trial. The controller responded to venous BG measured every five minutes using an FDA-approved GlucoScout (International Biomedical), and commanded insulin–glucagon control doses. The doses were administered using FDA-approved Deltec CoZmo infusion pumps (Smiths Medical).

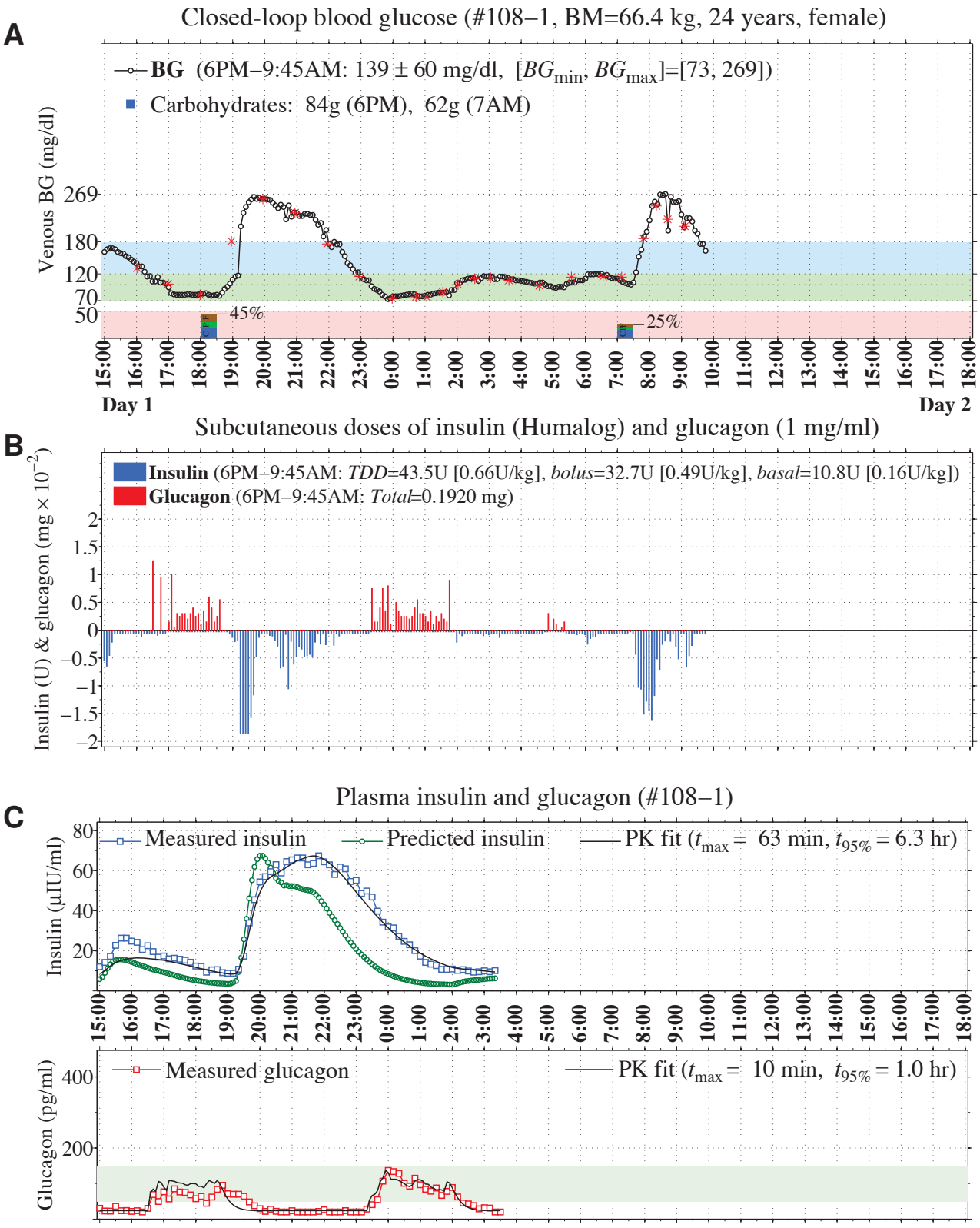

Fig. S2. First closed-loop experiment in #108 using controller with fast PK parameter settings, where no carbohydrate intervention was required. In this subject's case (and in Figs. S3–S7) the disparity between the subject's measured lispro PK and the model-estimated lispro PK predicted online by the controller using fast PK parameter settings was not as large as in subjects with carbohydrate-requiring hypoglycemia (Figs. S8–S12). In this subject's case, blood samples obtained after 3:20 on the second day were determined to be hemolyzed. Both the main and blood-sparing IV lines failed before 10:00 on the second day (the main IV line failed after a total of 15.75 hours past 18:00 on admission day). Note, meals are indicated by multicolored rectangles, where blue indicates carbohydrate (C), green indicates protein (P), and brown indicates fat (F); the height of each rectangle is proportional to the total daily macronutrient content (indicated by percentages). See caption for Fig. 1A in main paper.

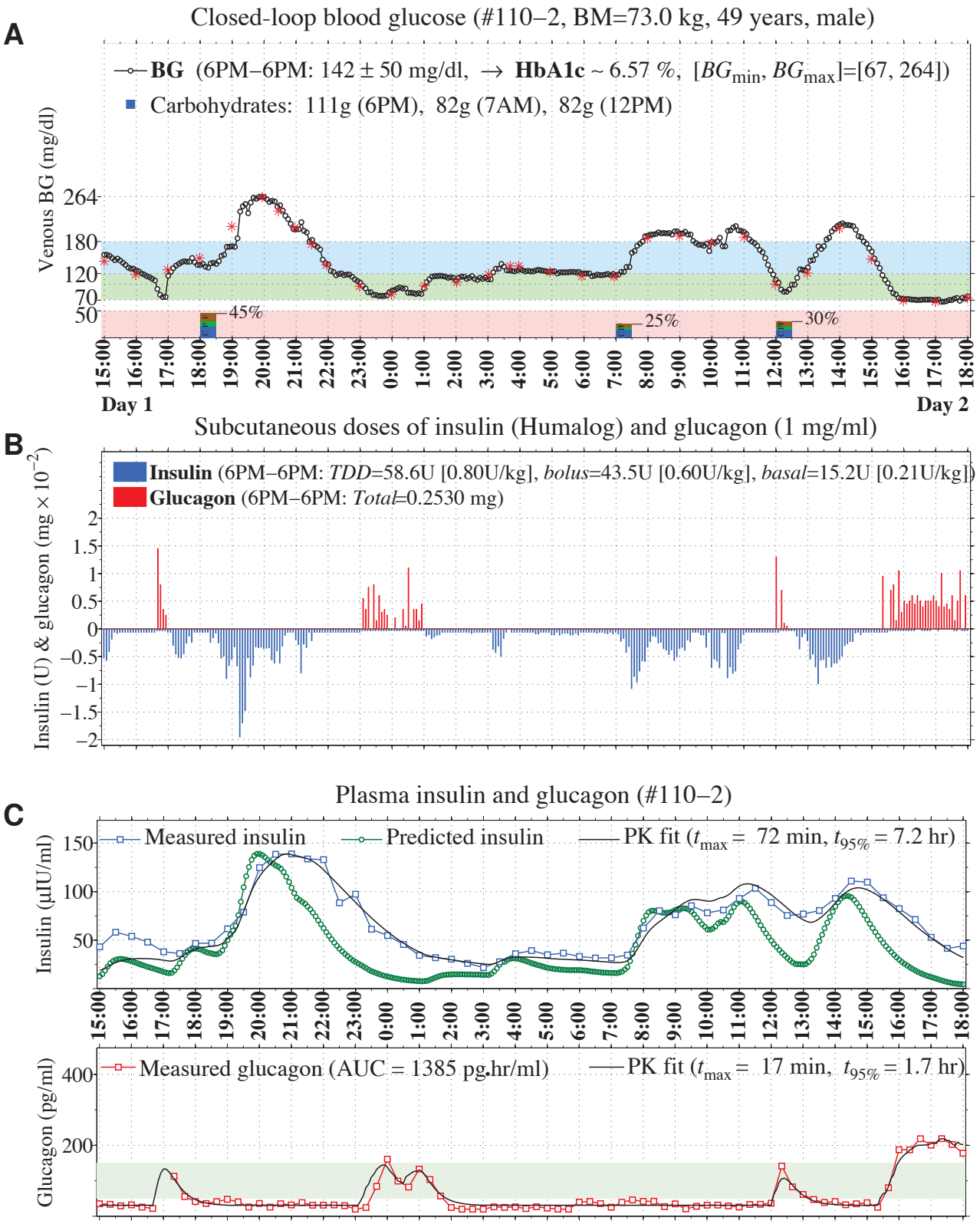

Fig. S3. First closed-loop experiment in #110 using controller with fast PK parameter settings, where no carbohydrate intervention was required.

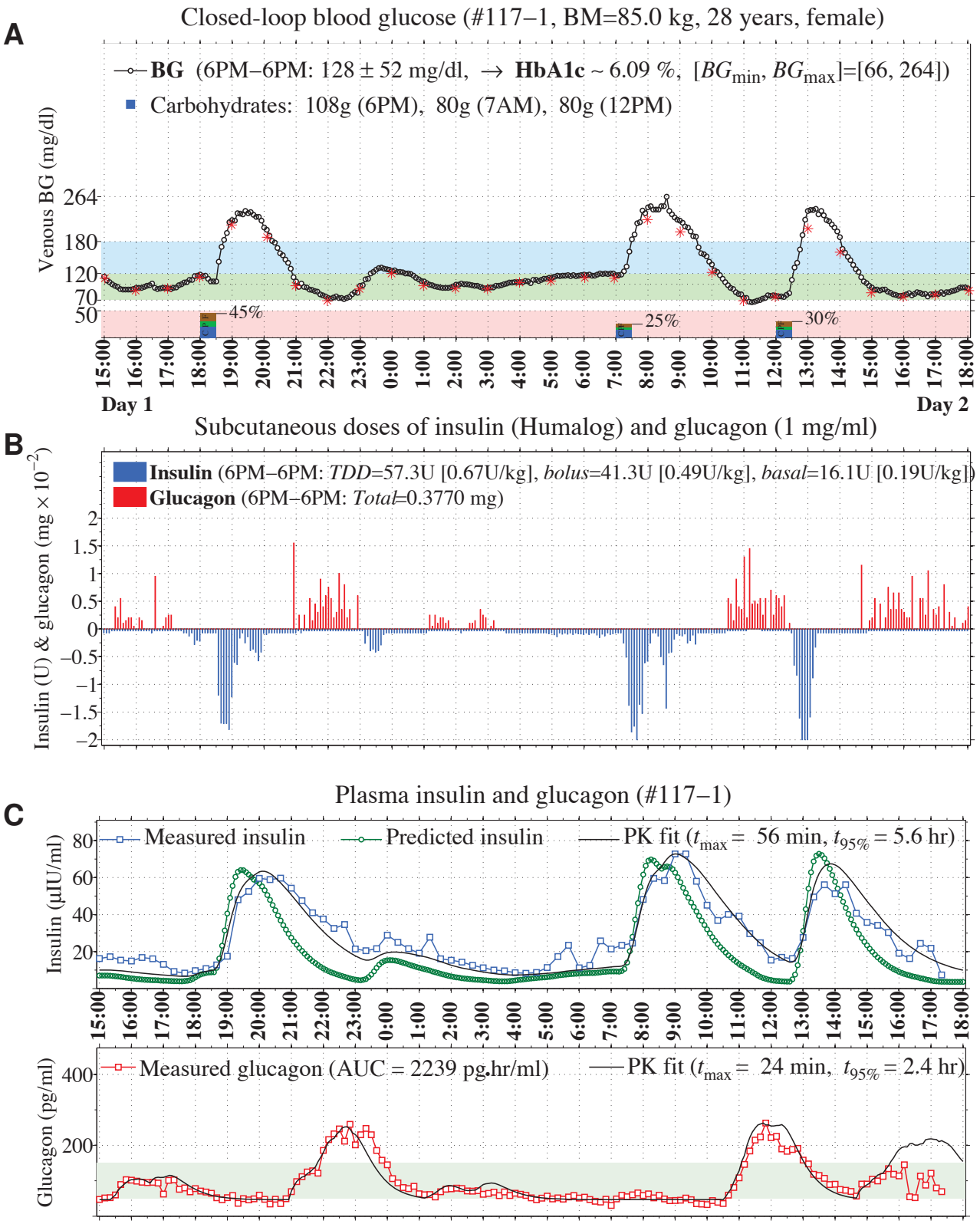

Fig. S4. First closed-loop experiment in #117 using controller with fast PK parameter settings, where no carbohydrate intervention was required.

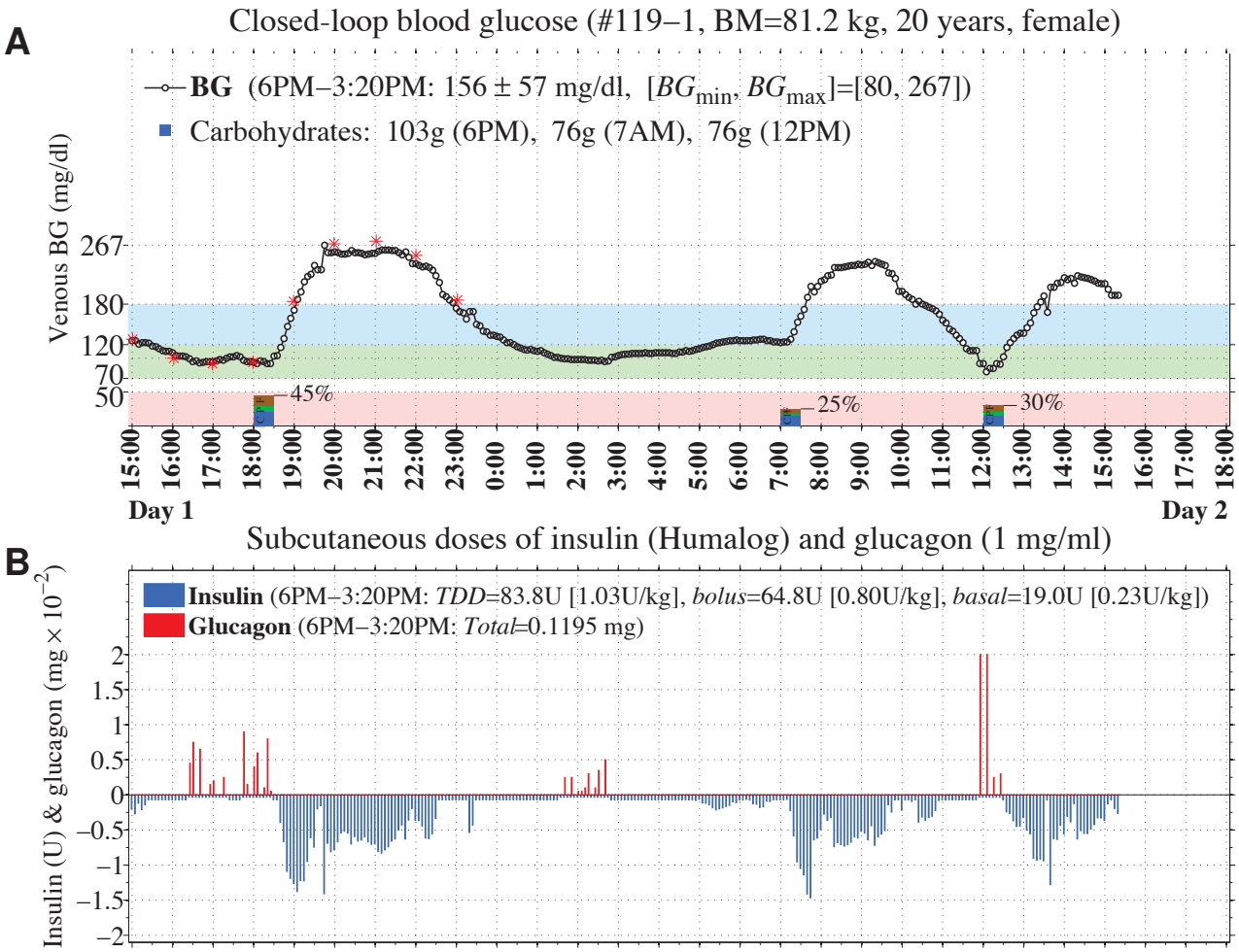

Fig. S5. First closed-loop experiment in #119 using controller with fast PK parameter settings, where no carbohydrate intervention was required. In this subject's case, blood samples were determined to be hemolyzed. The blood-sparing line failed shortly after 23:00 on admission day and the experiment was discontinued at 15:20 on the second day due to failure of the main IV line (a total of 21.33 hours past 18:00 on admission day).

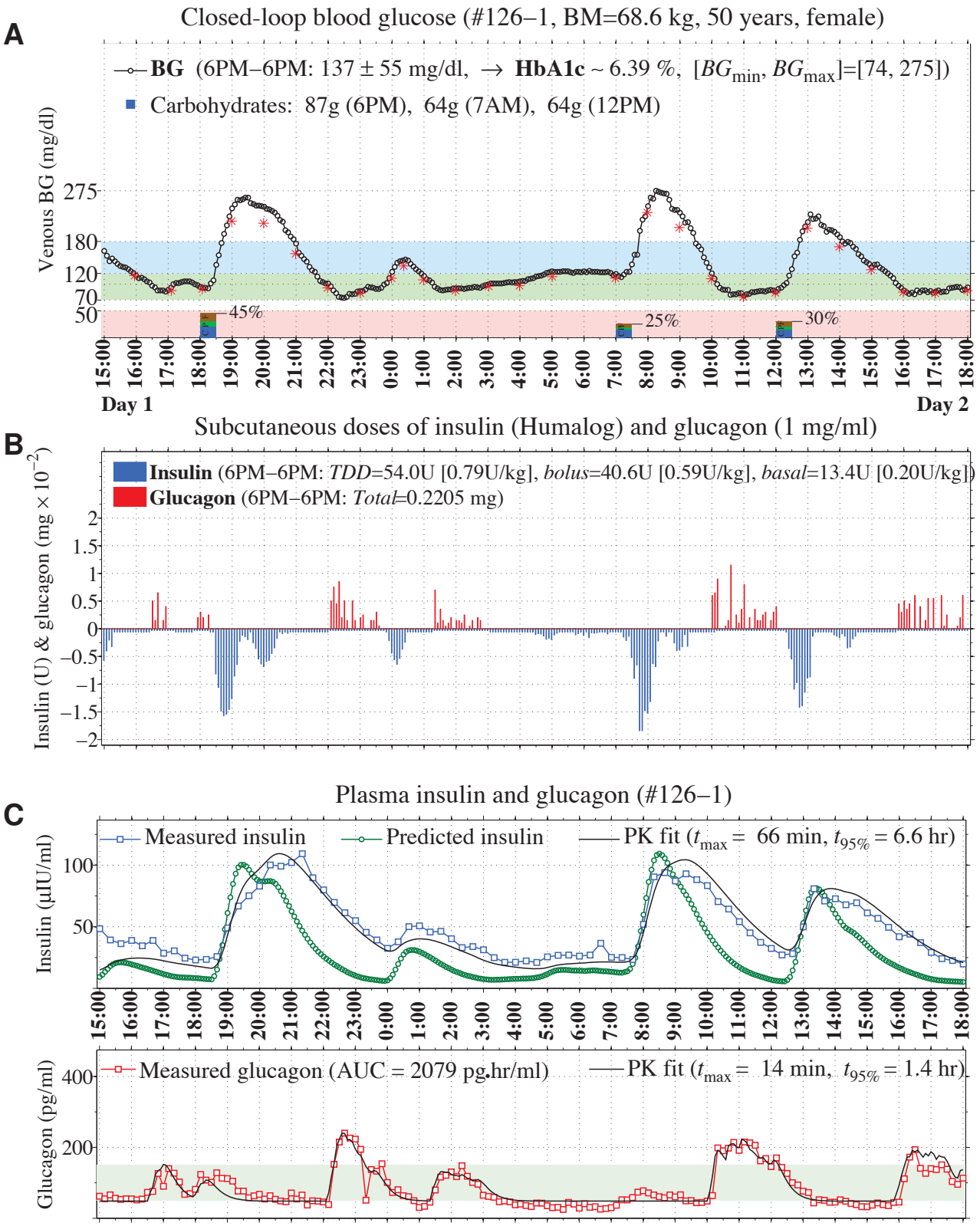

Fig. S6. First closed-loop experiment in #126 using controller with fast PK parameter settings, where no carbohydrate intervention was required.

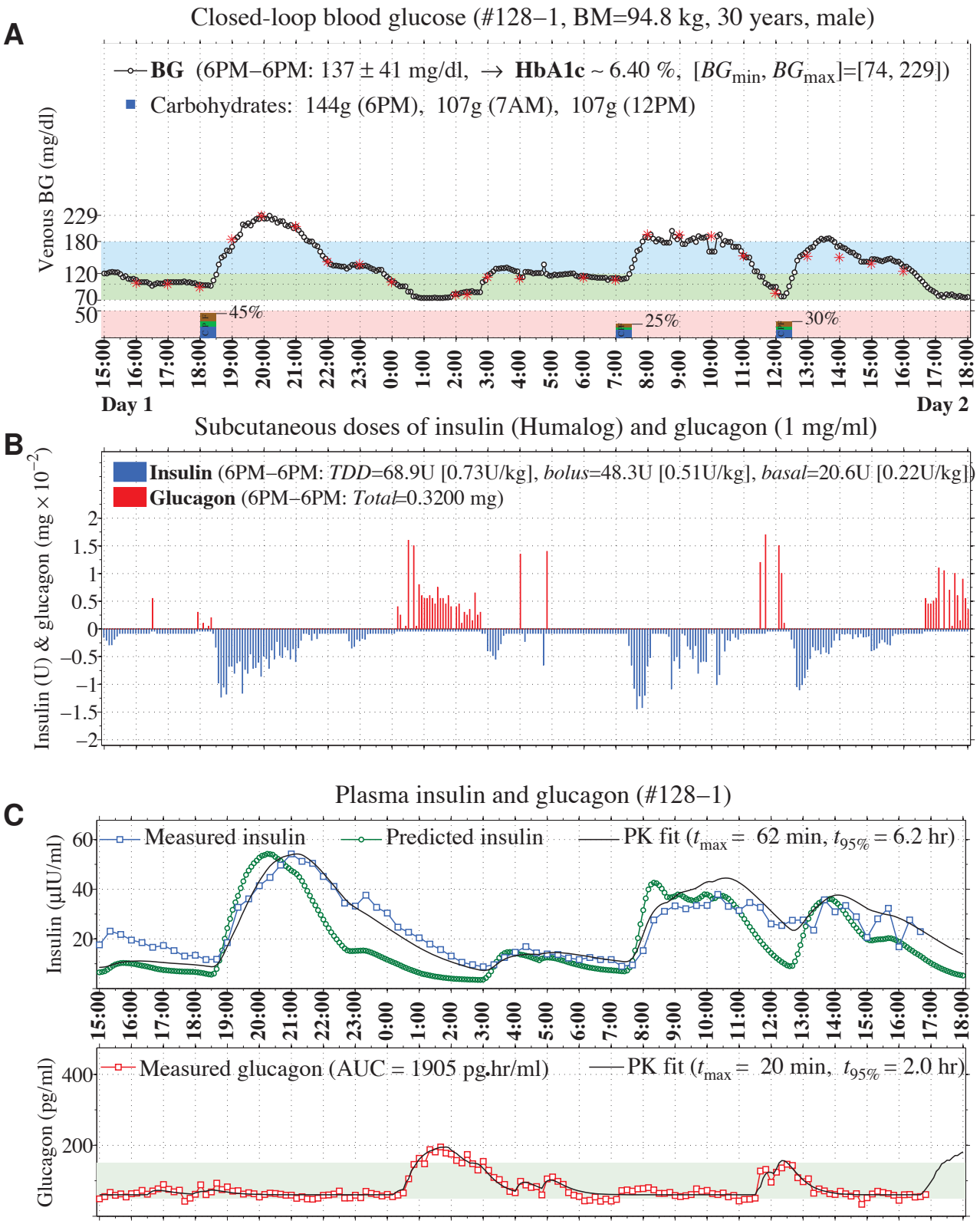

Fig. S7. First closed-loop experiment in #128 using controller with fast PK parameter settings, where no carbohydrate intervention was required.

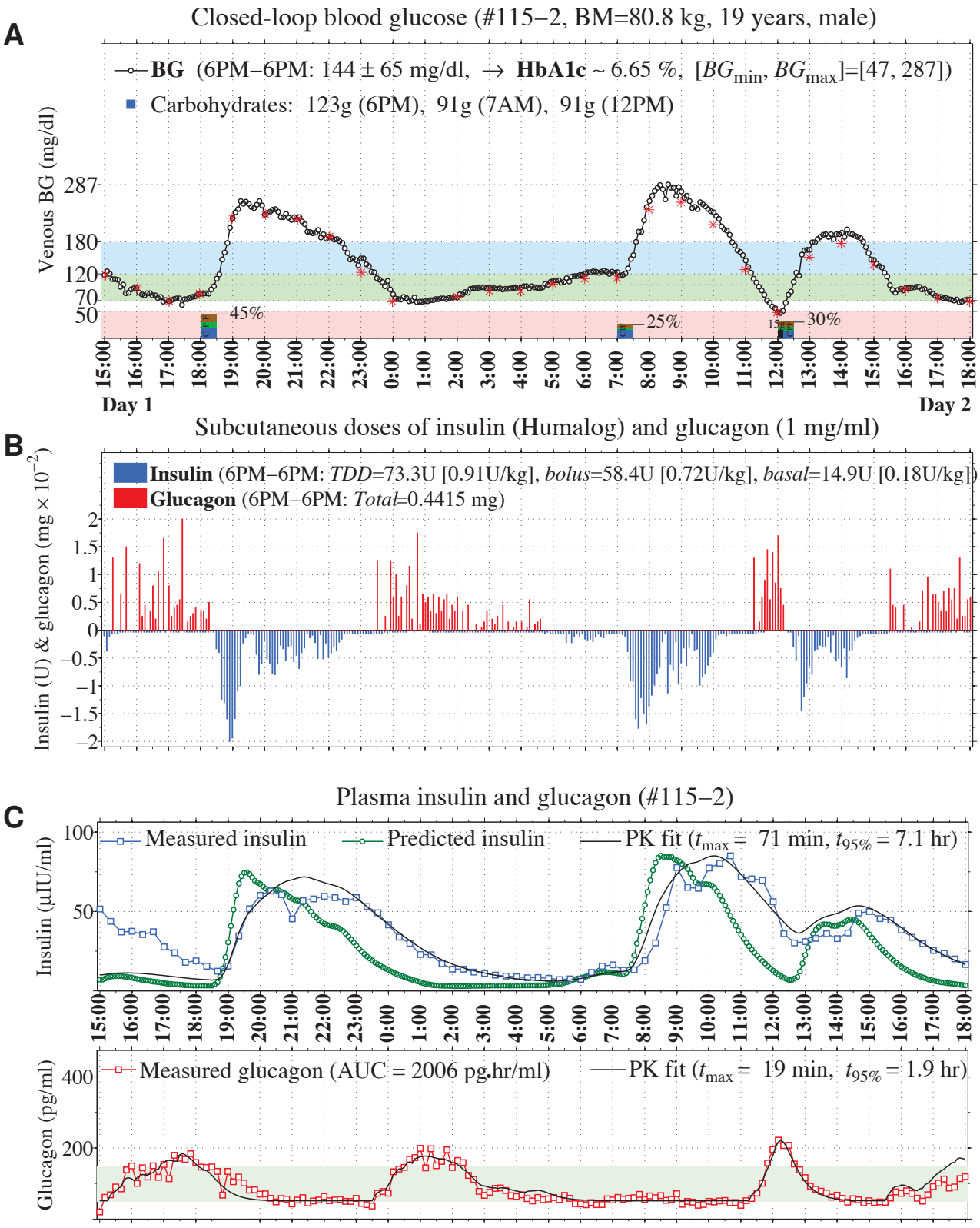

Fig. S8. First closed-loop experiment in #115 using controller with fast PK parameter settings, where carbohydrate intervention was required. In this subject's case (and in Figs. S9–S12), the disparity between measured lispro PK in this subject and the online PK prediction by the controller using fast PK parameter settings (C) led to an excessively high lispro concentration in the late post-prandial period, which resulted in hypoglycemia apparently refractive to micro-doses of glucagon. Consequently, carbohydrate intervention was required. Note, carbohydrate intervention (15 g) is indicated along the timeline in (A) by a black rectangle.

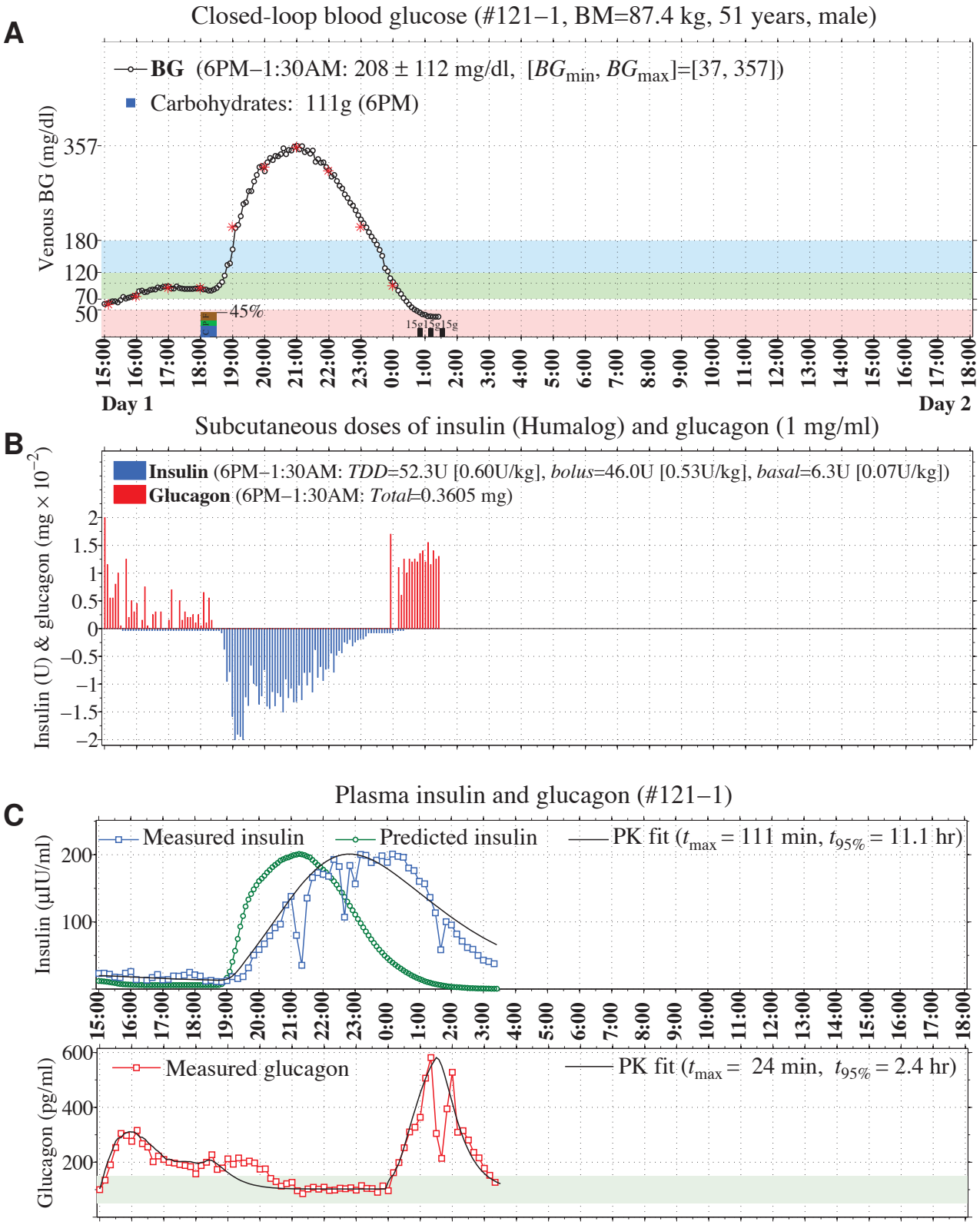

Fig. S9. First closed-loop experiment in #121 using controller with fast PK parameter settings, where carbohydrate intervention was required. In this subject's case, closed-loop control was discontinued at 1:30 on the second day after intervention with IV dextrose (a total of 7.5 hours past 18:00 on admission day).

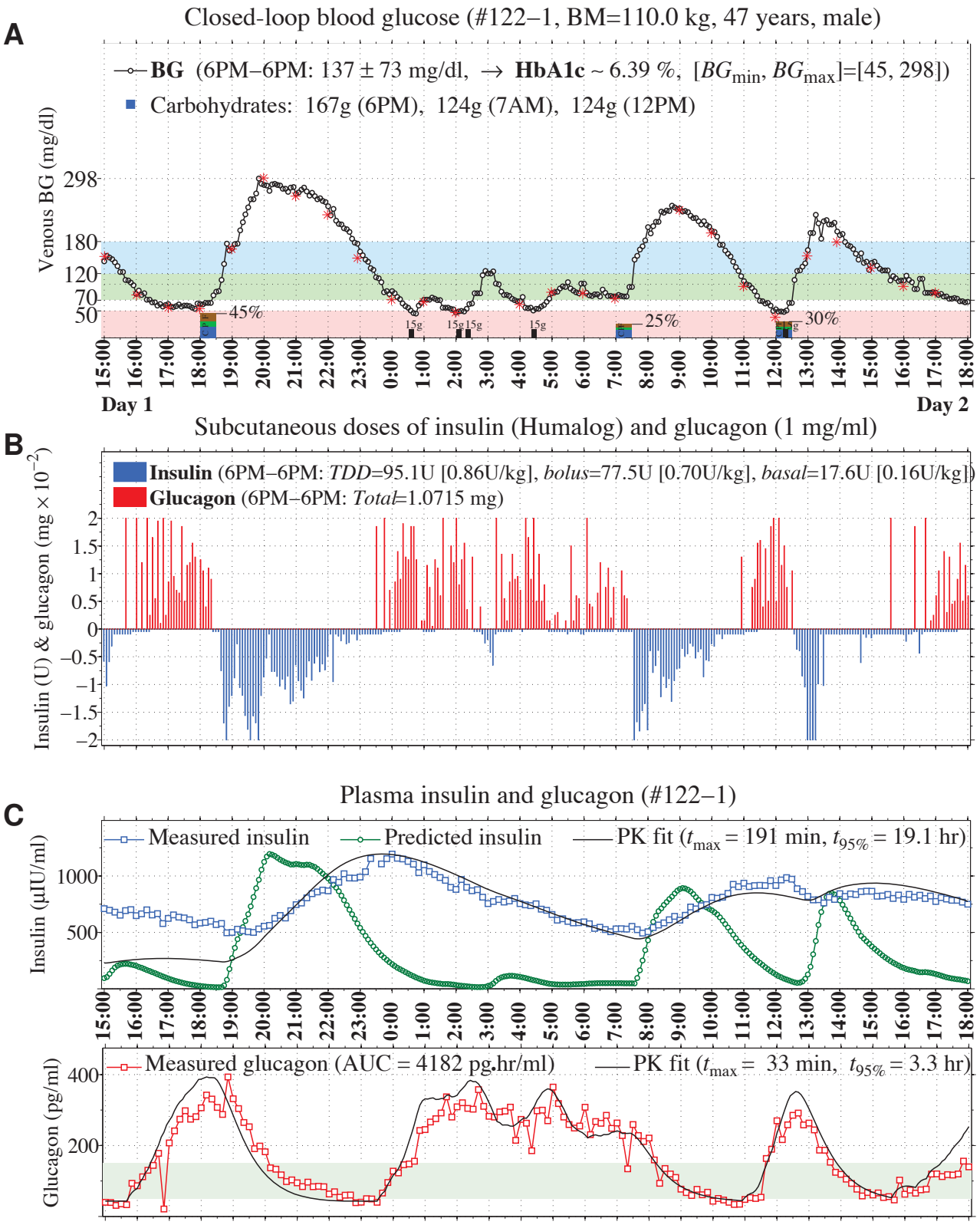

Fig. S10. First closed-loop experiment in #122 using controller with fast PK parameter settings, where carbohydrate intervention was required.

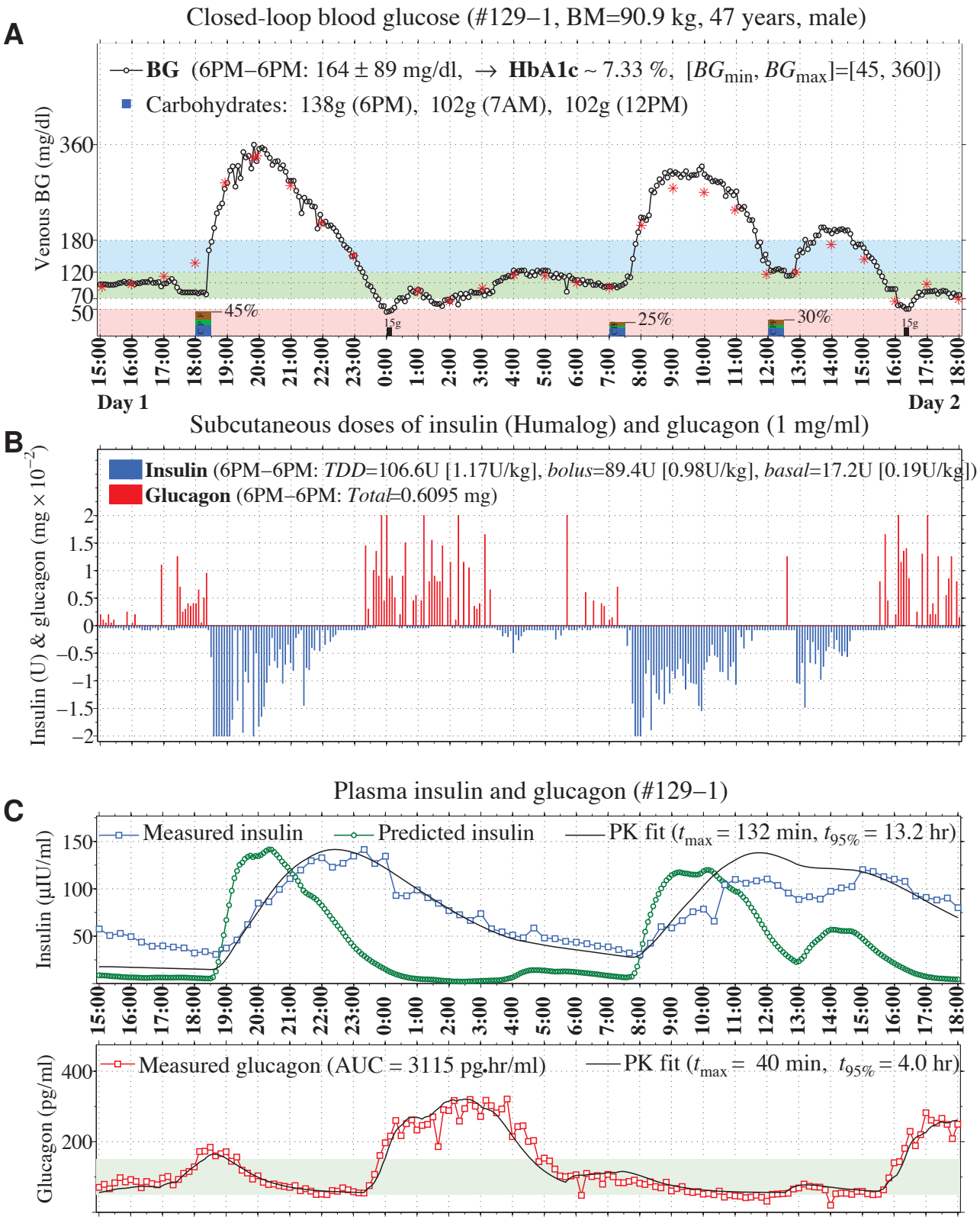

Fig. S11. First closed-loop experiment in #129 using controller with fast PK parameter settings, where carbohydrate intervention was required.

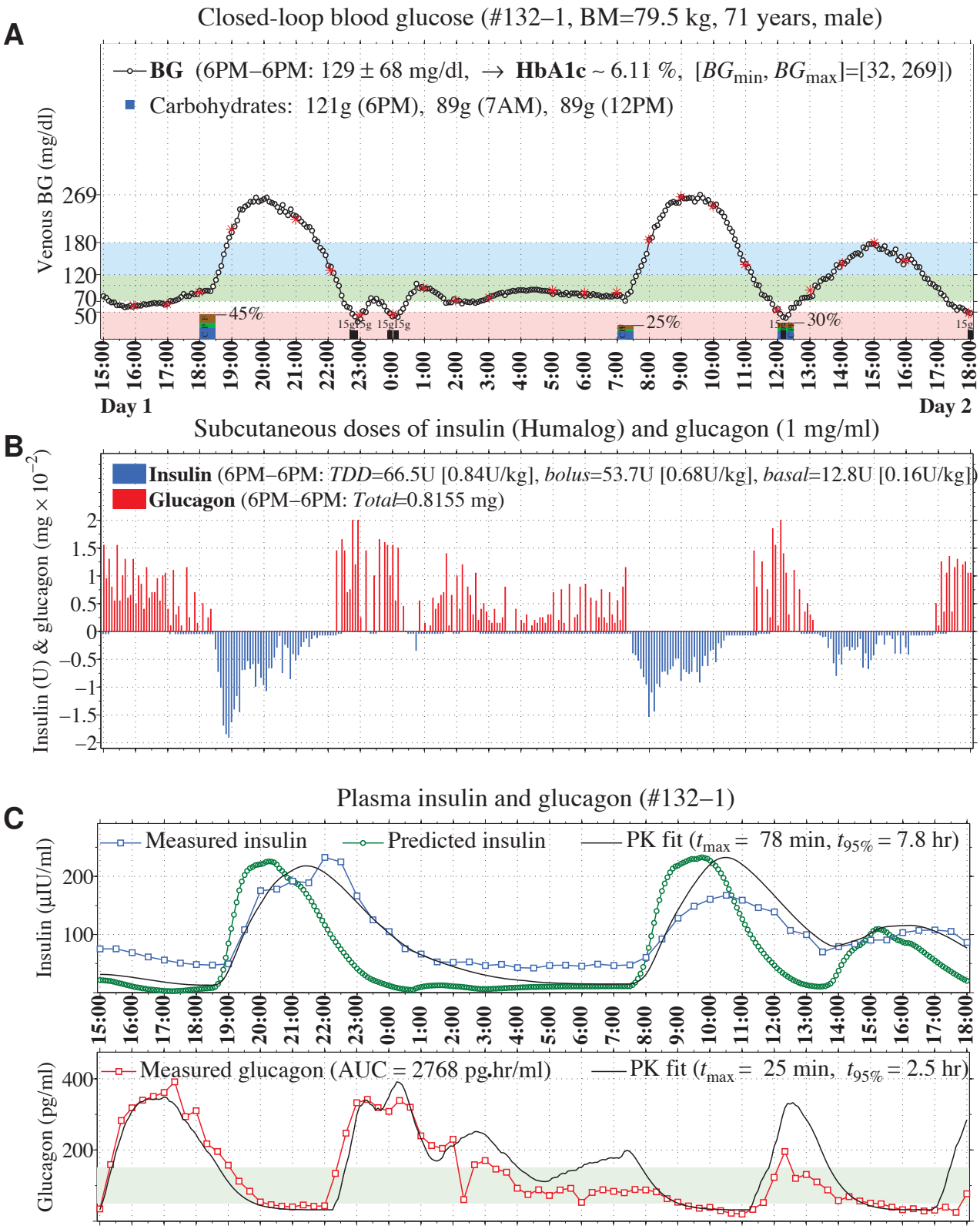

Fig. S12. First closed-loop experiment in #132 using controller with fast PK parameter settings, where carbohydrate intervention was required.

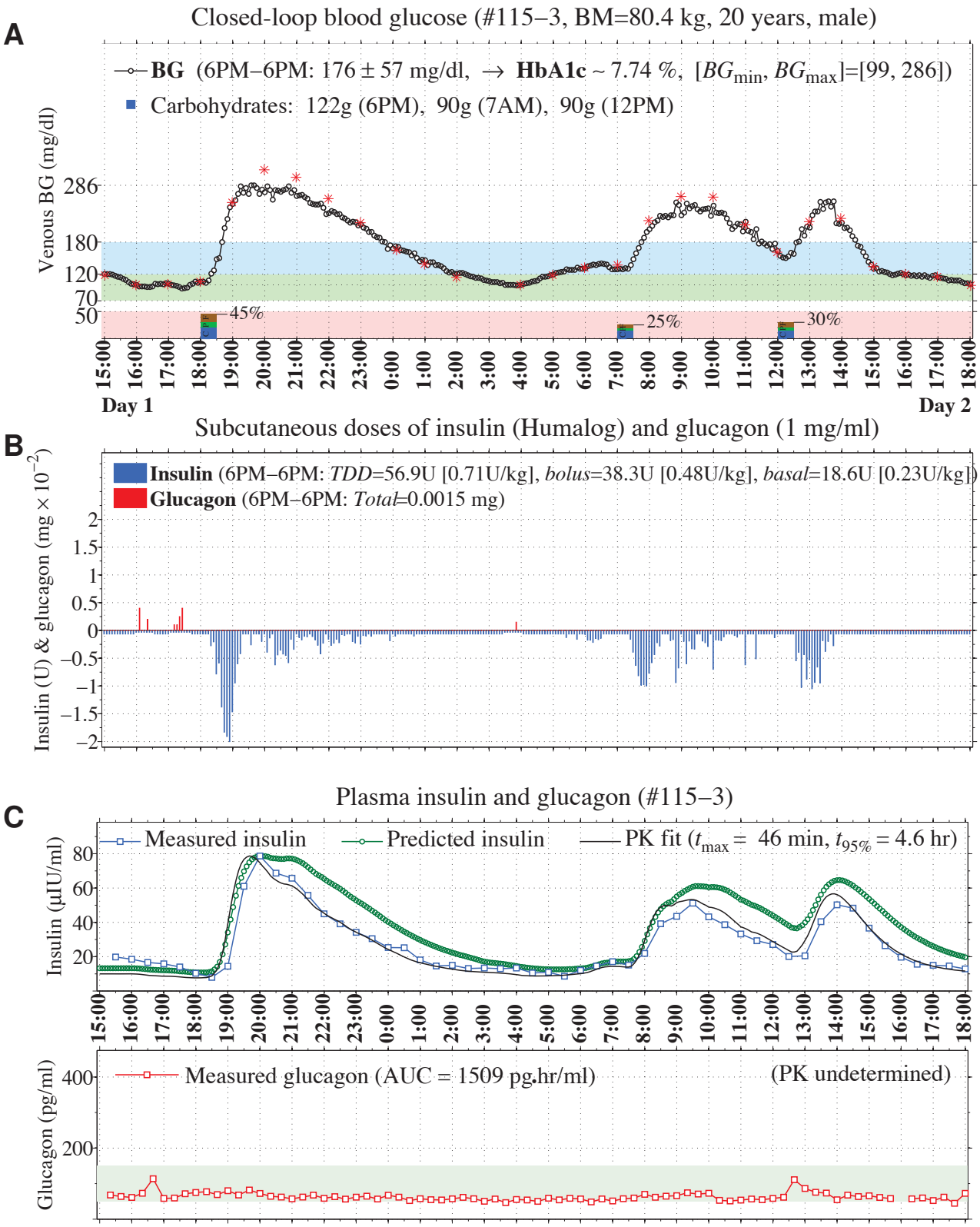

Fig. S13. Second closed-loop experiment in #115 using controller with slow PK parameter settings, where no carbohydrate intervention was required. In this subject's case (and in Figs. S14–S18) the slow PK parameter settings led to improved online insulin PK estimation by the controller, and no carbohydrate intervention was required.

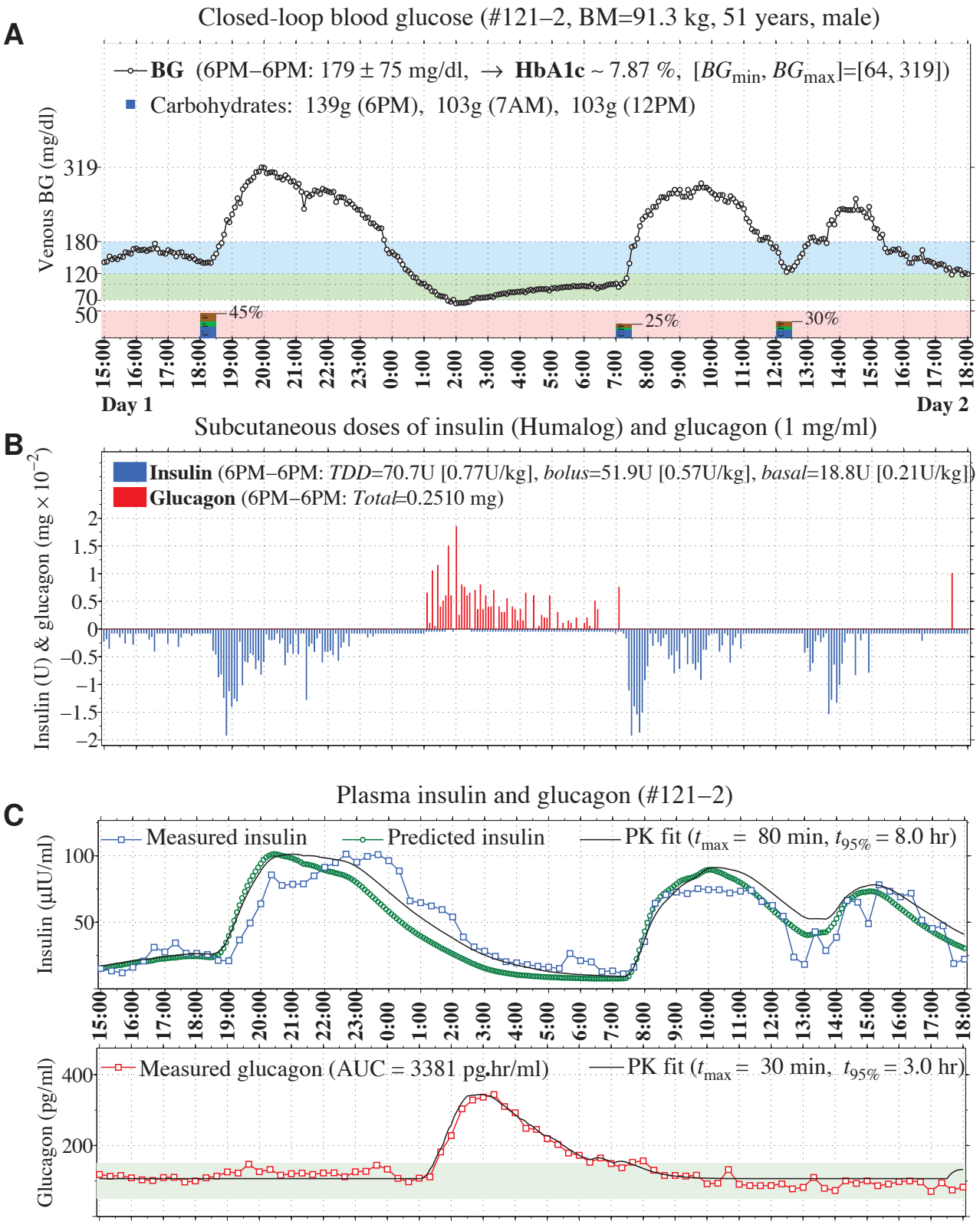

Fig. S14. Second closed-loop experiment in #121 using controller with slow PK parameter settings, where no carbohydrate intervention was required.

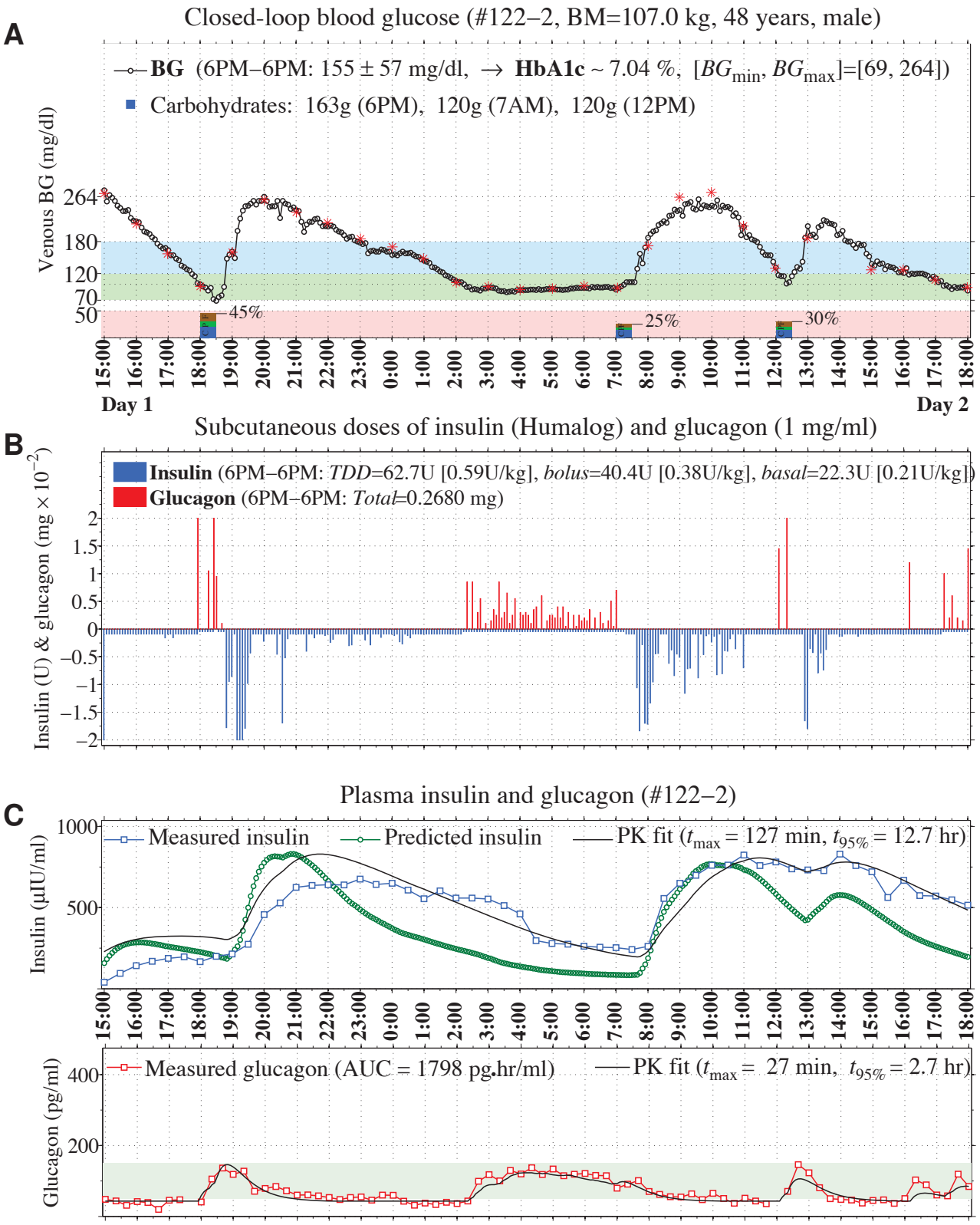

Fig. S15. Second closed-loop experiment in #122 using controller with slow PK parameter settings, where no carbohydrate intervention was required.

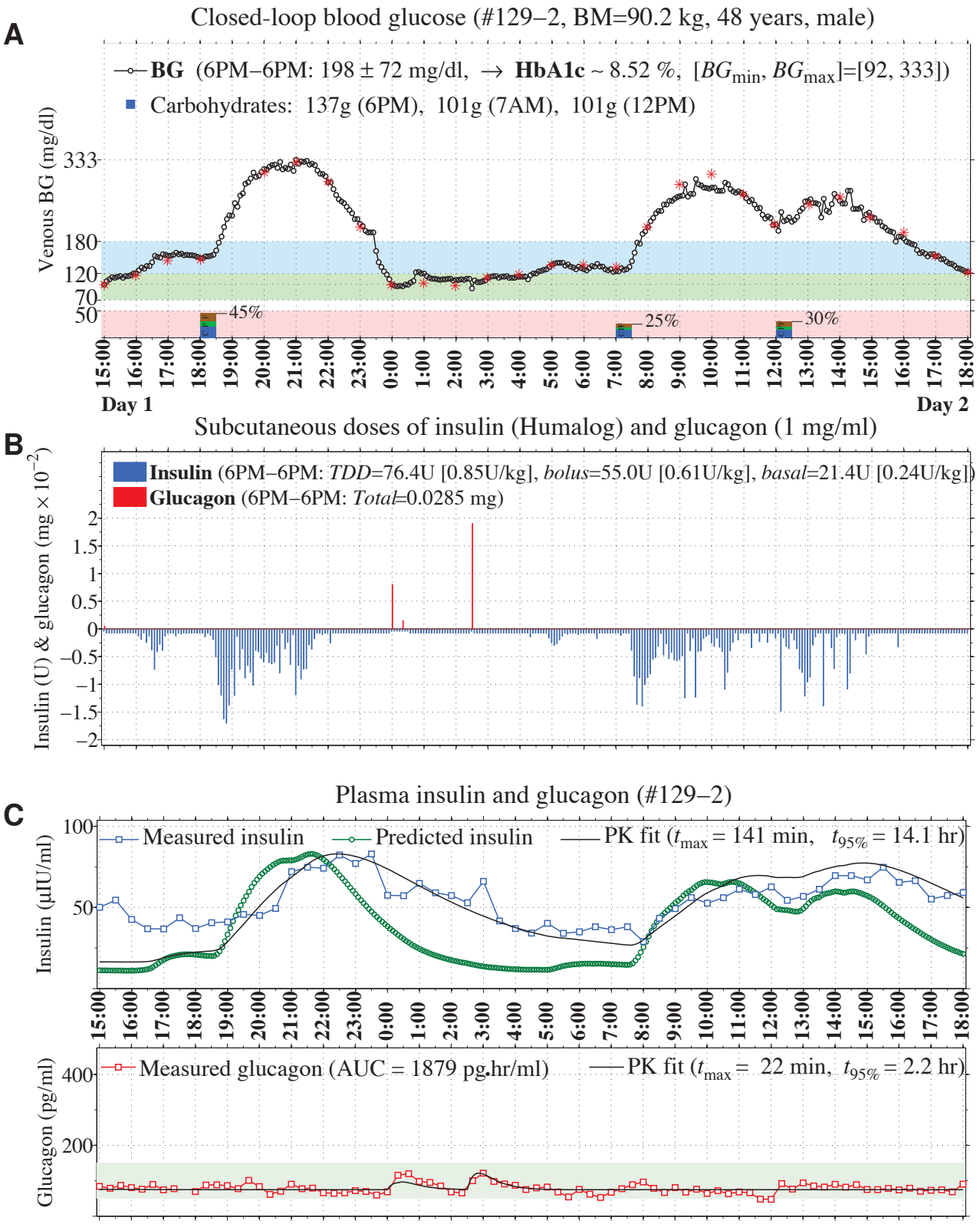

Fig. S16. Second closed-loop experiment in #129 using controller with slow PK parameter settings, where no carbohydrate intervention was required.

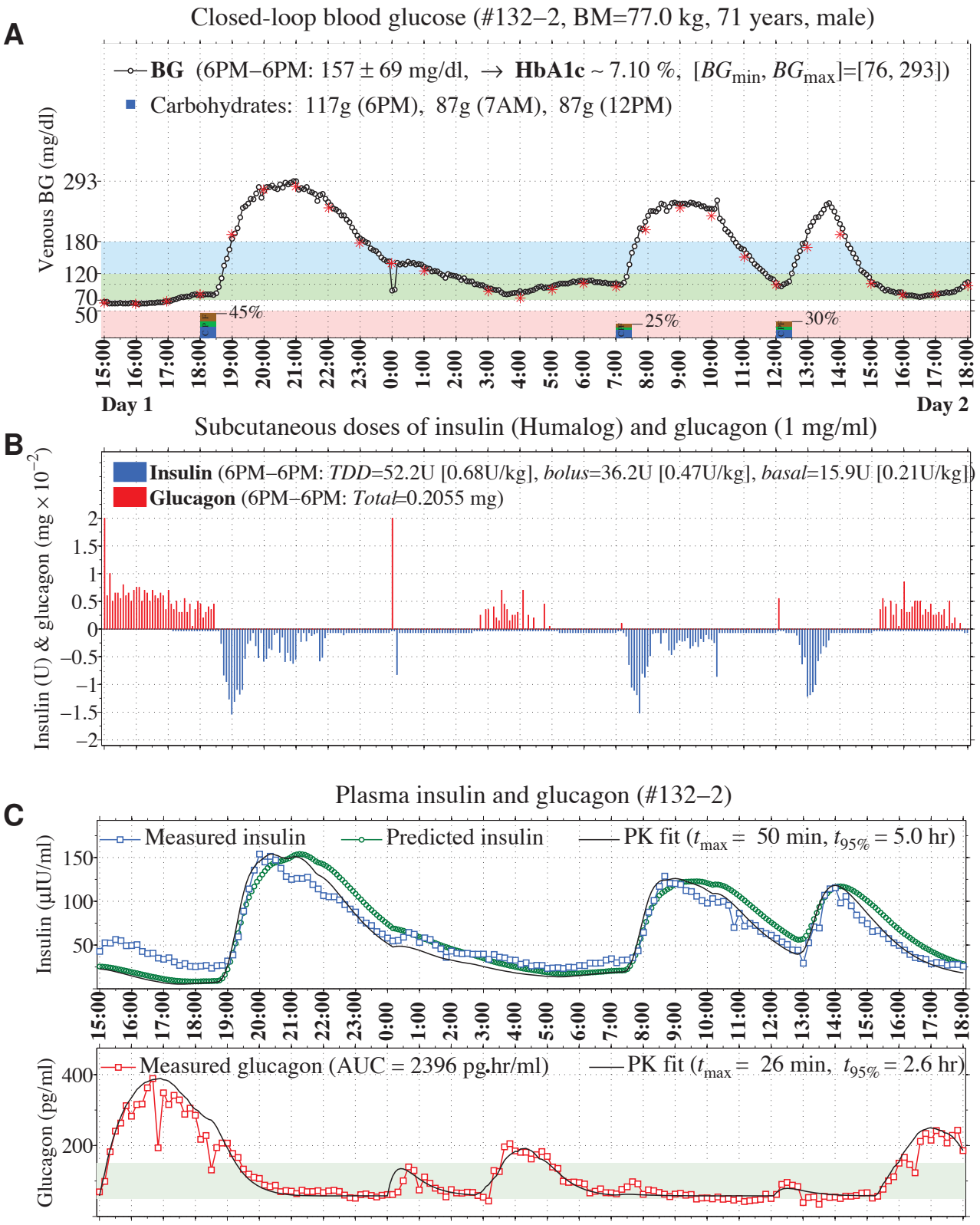

Fig. S17. Second closed-loop experiment in #132 using controller with slow PK parameter settings, where no carbohydrate intervention was required.

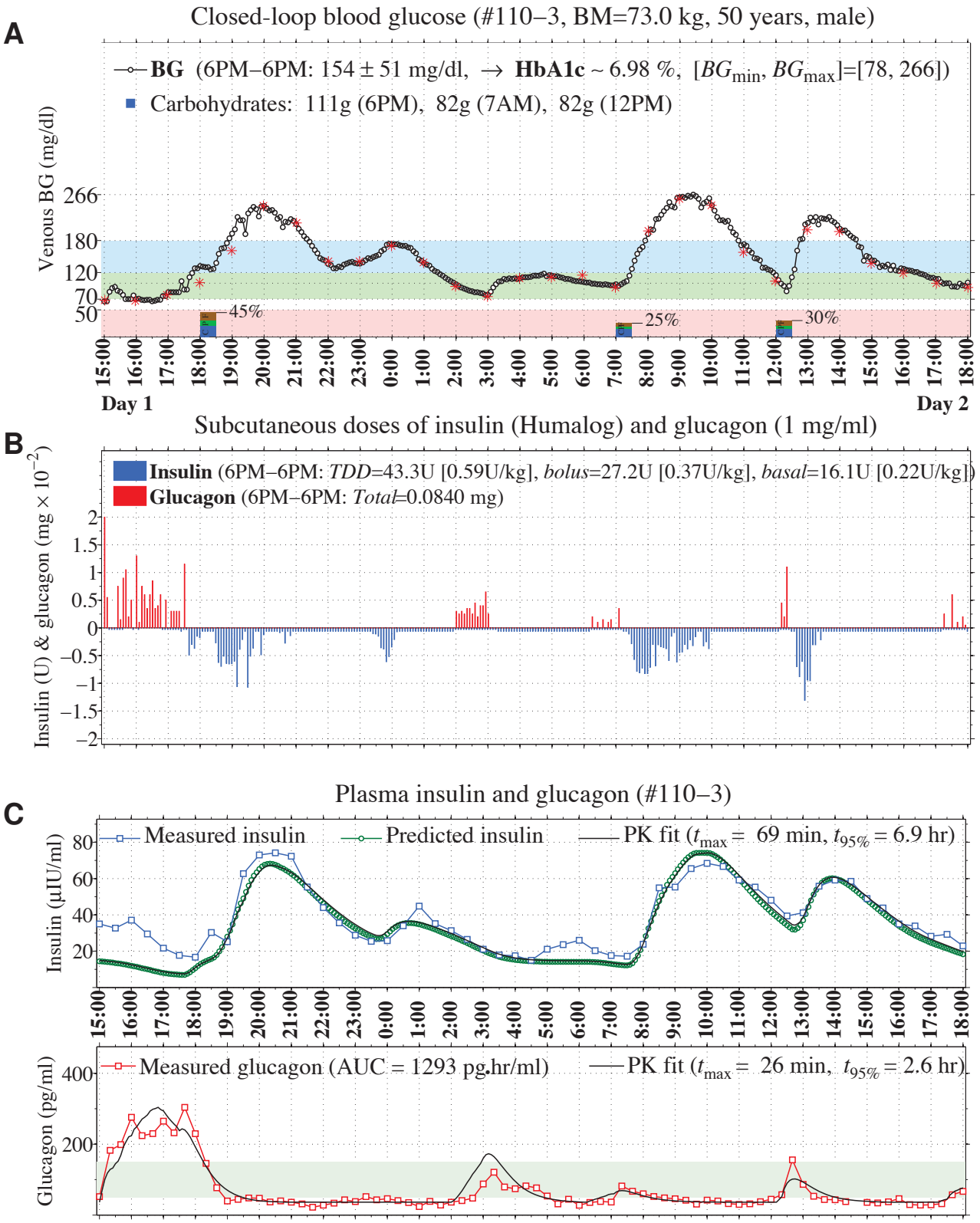

Fig. S18. Second closed-loop experiment in #110 using controller with slow PK parameter settings, where no carbohydrate intervention was required. In this subject's case (and in Figs. S19–21) the first experiment revealed a relatively fast lispro PK and did not require carbohydrate intervention. In this repeat experiment, where the control algorithm used slow PK parameter settings, no hypoglycemia occurred and there was only a minimal increase in mean BG relative to the first experiment.

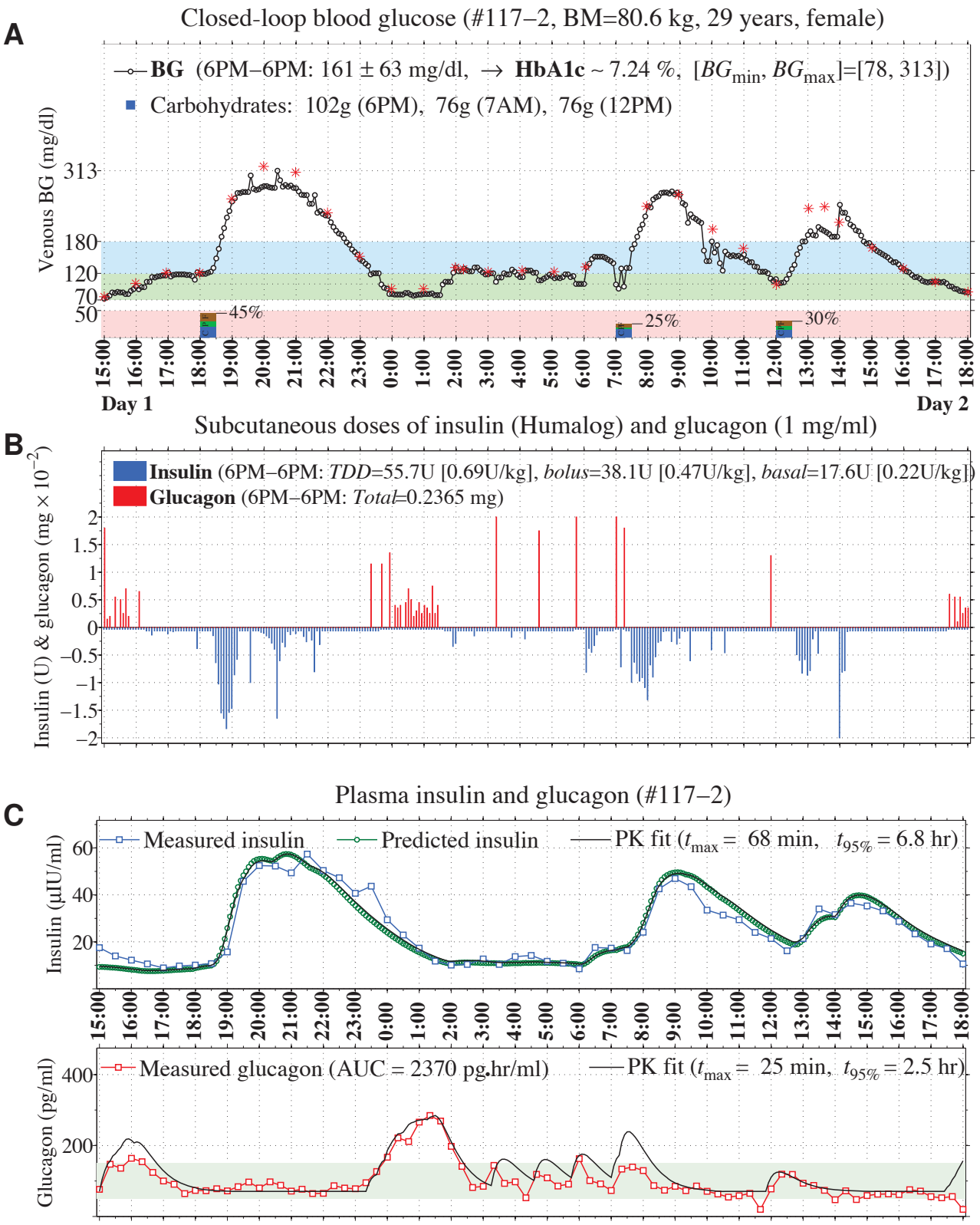

Fig. S19. Second closed-loop experiment in #117 using controller with slow PK parameter settings, where no carbohydrate intervention was required.

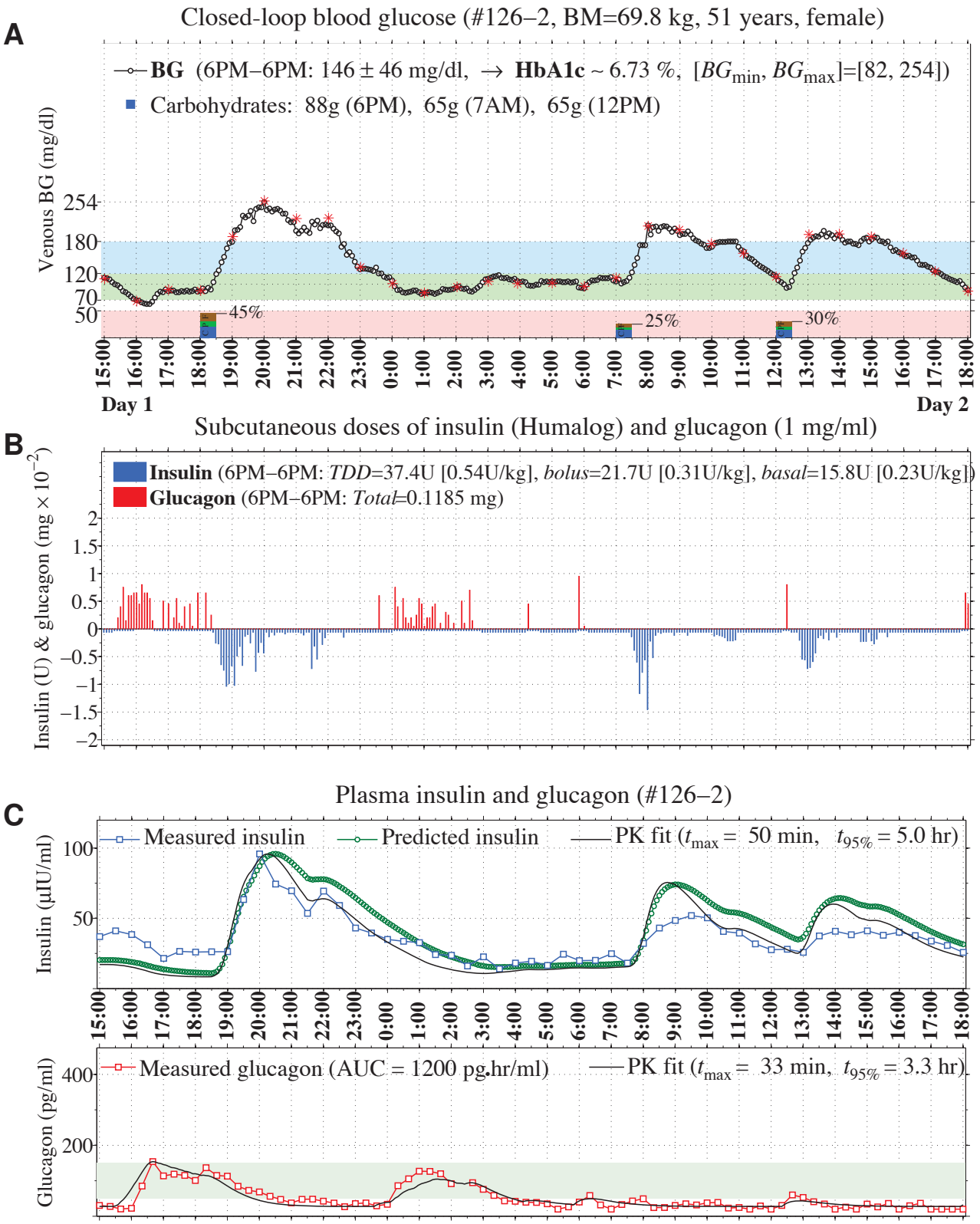

Fig. S20. Second closed-loop experiment in #126 using controller with slow PK parameter settings, where no carbohydrate intervention was required.

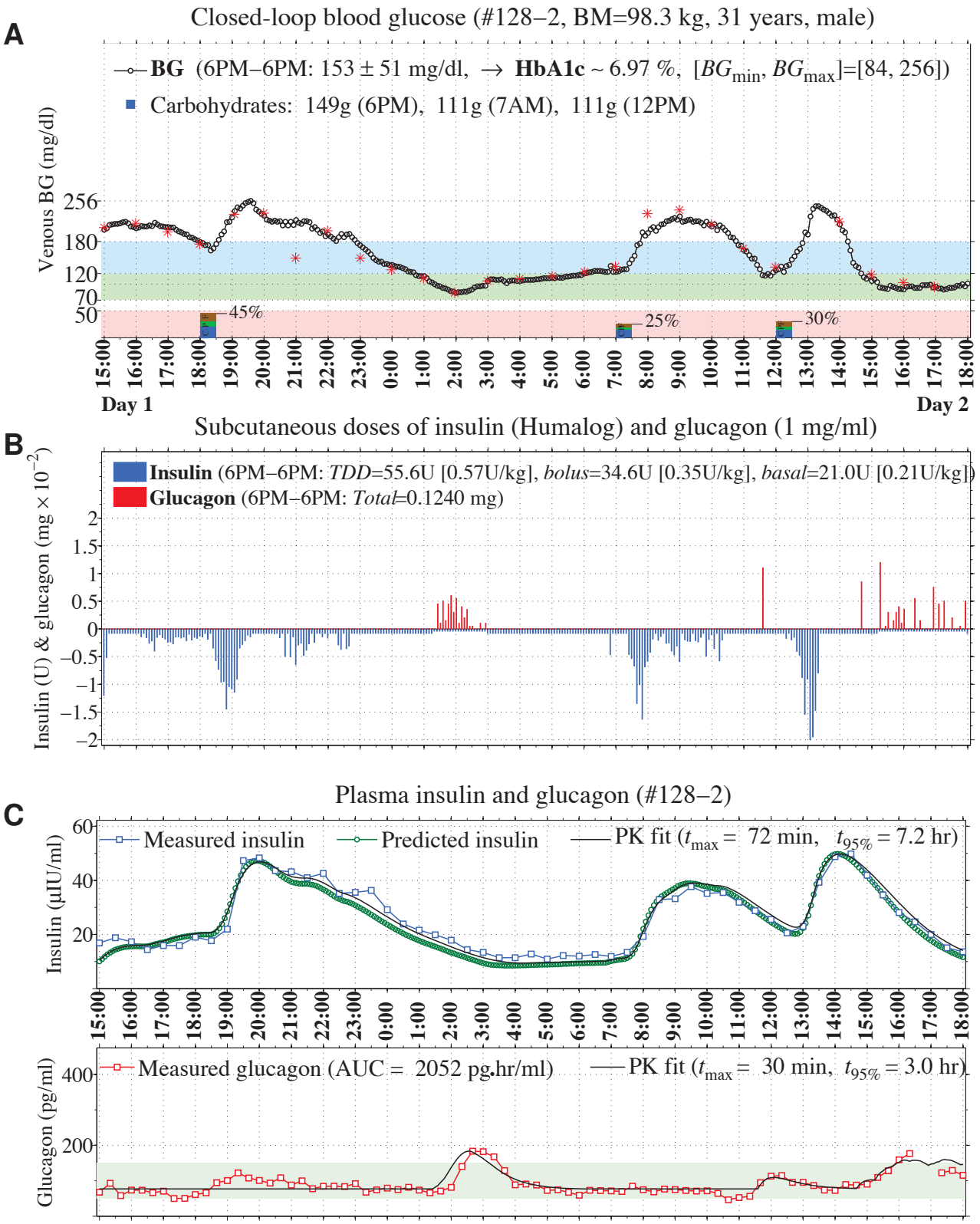

Fig. S21. Second closed-loop experiment in #128 using controller with slow PK parameter settings, where no carbohydrate intervention was required.

REFERENCES AND NOTES

1. F. H. El-Khatib, System identification and adaptive closed-loop glucose control in a type 1 diabetic swine model. *Ph.D. Dissertation*, Mechanical & Industrial Engineering Department, University of Illinois at Urbana-Champaign (2005).

2. K. J. Astrom, B. Wittenmark, On self-tuning regulators. *Automatica*, **9**, 195–199 (1973).

3. D. W. Clarke, P. J. Gawthrop, Self-tuning control. *Proc. IEEE*, **126**, 633–640 (1979).

4. U. Fischer, W. Schenk, E Salzsieder, G. Albrecht, P. Abel, and E.-J. Freyse, Does physiological blood glucose control require an adaptive control strategy? *IEEE Trans. Biomed. Eng.*, **BME-34**, 575–582 (1987).

5. T. L. Lai, C. Z. Wei, Extended least squares and their applications to adaptive control and prediction in linear systems. *IEEE Trans. Auto. Control*, **AC-31**, 898–906 (1986).

6. L. Ljung *System Identification: Theory for the user*, Prentice Hall (1999).

7. E. F. Comacho, C. Bordons, *Model Predictive Control*, Springer-Verlag (1979).

8. D. W. Clarke, C. Mohtadi, P. S. Tuffs, Generalized predictive control – Part I: the basic algorithm. *Int. J. Automatica*, **23**, 137–148 (1987).

9. C. E. Garcia, D. M. Prett, M. Morari, Model predictive control: Theory and practice – A survey. *Automatica*, **25**, 335–348 (1989).

10. L. Guo, Further results on least squares based adaptive minimum variance control. *SIAM J. Control Optim.*, **32**, 187–212 (1994).

11. S. L. Noble, E. Johnston, B. Walton, Insulin lispro: a fast-acting insulin analog. *Am.& Fam. Physician*, **5**, 279–292 (1998).

12. As such, for an impulse dose U_0, $p(0) = 0$ and $p(t \to \infty) = 0$.

13. A. Plum, H. Agerso, L. Andersen, Pharmacokinetics of the rapid-acting insulin analog, insulin aspart, in rats, dogs, and pigs, and pharmacodynamics of insulin aspart in pigs. *Drug Metab. Disposition*, **28**, 155–160 (2000).

14. F. H. El-Khatib, J. Jiang, R. G. Gerrity, E. R. Damiano, Pharmacodynamics and stability of subcutaneously infused glucagon in a type 1 diabetic swine model *in vivo*. *Diabetes Technol. Therap.*, **9**, 135–144 (2007).

15. F. H. El-Khatib, J. Jiang, E. R. Damiano, Adaptive closed-loop control provides blood-glucose regulation using dual subcutaneous insulin and glucagon infusion in diabetic swine. *J. Diabetes Sci. Technol.*, **2**, 181–192 (2007).

16. F. H. El-Khatib, J. Jiang, E. R. Damiano, A feasibility study of bihormonal closed-loop blood glucose control using dual subcutaneous infusion of insulin and glucagon in ambulatory diabetic swine. *J. Diabetes Sci. Technol.*, **3**, 789–803 (2009).